Microbialites in Last Glacial Maximum and deglacial reefs of the Great Barrier Reef (IODP Expedition 325, NE Australia)

Juan C. Braga[a,*], Ángel Puga-Bernabéu[a], Katrin Heindel[b,1], Madhavi A. Patterson[c], Daniel Birgel[d], Jörn Peckmann[d], Isabel M. Sánchez-Almazo[e], Jody M. Webster[c], Yusuke Yokoyama[f], Robert Riding[g]

[a] Departamento de Estratigrafía y Paleontología, Universidad de Granada, Campus Fuentenueva, 18002 Granada, Spain
[b] Department für Geodynamik und Sedimentologie, Universität Wien, Althanstrasse 14, A-1090 Wien, Austria
[c] Geocoastal Research Group, School of Geosciences, The University of Sydney, Sydney, NSW 2006, Australia
[d] Institut für Geologie, Centrum für Erdsystemforschung und Nachhaltigkeit, Universität Hamburg, 20146 Hamburg, Germany
[e] Centro de Instrumentación Científica, Universidad de Granada, Campus Fuentenueva, 18002 Granada, Spain
[f] Atmosphere and Ocean Research Institute, University of Tokyo, 5-1-5 Kashiwanoha, Kashiwa, Chiba 277-8564, Japan
[g] Department of Earth and Planetary Sciences, University of Tennessee, Knoxville, TN 37996, USA

A R T I C L E   I N F O

A B S T R A C T

Microbialites are volumetrically abundant components in Last Glacial Maximum and deglacial reefs in the Australian Great Barrier Reef sampled by IODP Expedition 325 in 34 holes from 17 sites (M0030–M0058), along four transects on the shelf edge. Detailed radiometric datings show that four distinct reef phases developed between 28 and 10 ka, displaying offlapping and then backstepping patterns. The reef boundstone facies include coralgal, coralgal-microbialite and microbialite boundstone. The microbialite consists of combinations of micrite/microspar, bioclasts, siliciclastic grains (up to 14.5%), fenestrae and encrusting epibionts. The micrite/microspar is high-magnesian calcite commonly irregularly clotted, fenestral and peloidal. Mesoscale microbialite fabrics include laminated, structureless, digitate, intraskeletal and boring-filling, and coatings on debris. Intraskeletal and boring-filling is the first fabric to develop in skeletal voids and borings. It is usually followed by structureless and laminated microbialite, locally overlain by digitate fabric. Microbialite-coated debris can occur at any stage in this succession, including in bioclastic accumulations where the scarce in situ framework builders are mainly encrusting corals. Lipid biomarkers of intermediate to high specificity for sulfate-reducing bacteria, together with $\delta^{13}C$ values of these lipids, indicate that microbialite formation was favored by sulfate-reducing bacteria in anoxic microenvironments, probably under high nutrient levels. The microbialite in fore-reef deposits accumulated in the photic zone in water depths of a few to several tens of meters, within small spaces generated by large bioclasts and encrusting corals in the topmost centimeters of the sediment. These crusts that formed on the illuminated surface constitute a previously unrecognized style of microbialite formation in Quaternary reefs. As with the cryptic crusts described from other reef locations, its greatest development occurred during the Last Glacial Maximum and early deglaciation. Microbial carbonate formation during this interval may reflect elevated seawater carbonate saturation corresponding with relatively low levels of atmospheric CO_2.

1. Introduction

Non-skeletal carbonate crusts are locally common in late Quaternary Indo-Pacific and Caribbean tropical coral reefs (Montaggioni and Camoin, 1993; Camoin et al., 1999, 2006; Heindel et al., 2012). In shallow-water reefs, the crusts typically formed during late phases of framework building as veneers on corals and encrusting epibionts, and completely or partially filled empty spaces in the reef framework (Seard et al., 2011 and references therein). Similar crusts developed on deep fore-reef slope surfaces at depths of 80–200 m in widespread locations, overlying low-light framework encrusters such as deep-water corallines, and covered by pelagic sediments (Brachert and Dullo, 1991; Camoin et al., 2006; Webster et al., 2009; Riding, 2011a). Although non-skeletal crusts were initially interpreted as cements

---

(Macintyre, 1977, 1984; Marshall and Davies, 1981), they were shown to be essentially microbial carbonates in Holocene reefs in Tahiti (Montaggioni and Camoin, 1993; Cabioch et al., 1999a), as well as in other reef systems (southwestern Indian Ocean, Camoin et al., 1997; Vanuatu, Cabioch et al., 1998, 1999b), and on deep fore-reef slopes of several islands in the Pacific (Camoin et al., 2006; Webster et al., 2009). Microbial carbonates, often termed microbialites (Burne and Moore, 1987), are also common in older reefs throughout the Phanerozoic (Pratt, 1982; Riding et al., 1991; Webb, 1996; Riding and Tomás, 2006; Riding, 2011b).

Molecular and isotopic studies indicate that late Quaternary reefal microbialites were produced by heterotrophic bacterial communities (Pigott and Land, 1986; Camoin et al., 1999; Reitner et al., 2000), in which sulfate-reducing bacteria played a prominent role (Heindel et al., 2010, 2012). They form in anoxic microenvironments in which organic matter (EPS, coral mucus, marine snow) degradation within microbial mats promotes carbonate precipitation (Camoin et al., 1999; Heindel et al., 2012). Profuse development of these microbialites has been related to high nutrient levels (Camoin et al., 1999, 2006; Heindel et al., 2012), linked by some authors to fertilization of reef environments by runoff from volcanic islands (Camoin et al., 1999; Cabioch et al., 2006). Late Quaternary microbialite crusts are common in deglacial reefs but declined in thickness about 6000 (Camoin et al., 1999) or 10,000–12,000 (Riding et al., 2014) years ago. This pattern has been attributed to decreasing upwelling and terrestrial runoff, and subsequent reduction in nutrient availability in shallow waters, as sea level stabilized after deglaciation (Camoin et al., 1999). However, similarities between the trends of microbialite decline and calculated pH and carbonate saturation in tropical surface waters over the past 14 ka, suggest that crust decline could mainly be a result of natural ocean acidification due to deglacial increase in atmospheric CO_2 level (Riding et al., 2014).

The purpose of this paper is to describe and interpret microbialites associated with LGM and deglacial reef deposits in the Australian Great Barrier Reef (GBR) recovered by IODP Expedition 325 in 2010 (Yokoyama et al., 2011) (Fig. 1). Analysis of the composition and distribution of microbial carbonate fabrics indicates the presence of two main types of microbialite deposit in successive reef phases: 1) microbialites that formed in enclosed framework cavities in shallow-water reef facies, similar to those in deglacial reefs in Tahiti and other Indo-Pacific and Caribbean locations; and 2) microbialite boundstones that formed on the sea floor and/or within the top few centimeters of the sediment in fore-reef settings, at water depths of a few to several tens of meters. The latter are the best developed microbial carbonates that formed during the LGM and early deglaciation in the GBR. They represent a previously unrecognized context of microbialite formation in Quaternary reefs; quite distinct from the shallow-water framework and deep fore-reef slope microbialites described to date. The profuse development of these microbial crusts on the sea floor within the photic zone supports a strong connection between biogenically induced carbonate precipitation and elevated carbonate saturation of surface tropical seawater due to lower levels of atmospheric CO_2 during the LGM and initial deglaciation.

2. Methods

2.1. IODP drilling operations

IODP Expedition 325 drilled 34 holes, at 17 sites (M0030–M0058) along four transects, in three areas on the shelf edge of the Great Barrier Reef (Hydrographer's Passage, Noggin Pass and Ribbon Reef, Fig. 1). The holes were cored in water depths between 42 and 157 meters below sea level (mbsl), from a fossil barrier reef at 40–50 mbsl to a succession of terraces descending to the shelf break at ~120 mbsl where the sea floor grades into the upper slope (Abbey et al., 2011a; Webster et al., 2011). According to their morphology, depth and location, these features have been divided into inner, mid and outer terraces (Webster et al., 2011). Cores 6.6 cm in diameter were recovered from 42 to 211.7 mbsl, with an average of 26.6% recovery. Cores were cut into sections with 1.5 m maximum length. When two or more sites were drilled at the same coordinates, they are named using consecutive letters (e.g. M0054A and M0054B). In this study we focus on fossil coral-reef deposits from the two transects in which core recovery was highest: HYD-01C (M0031–39) off Mackay and NOG-01B (M0053A–57A) off
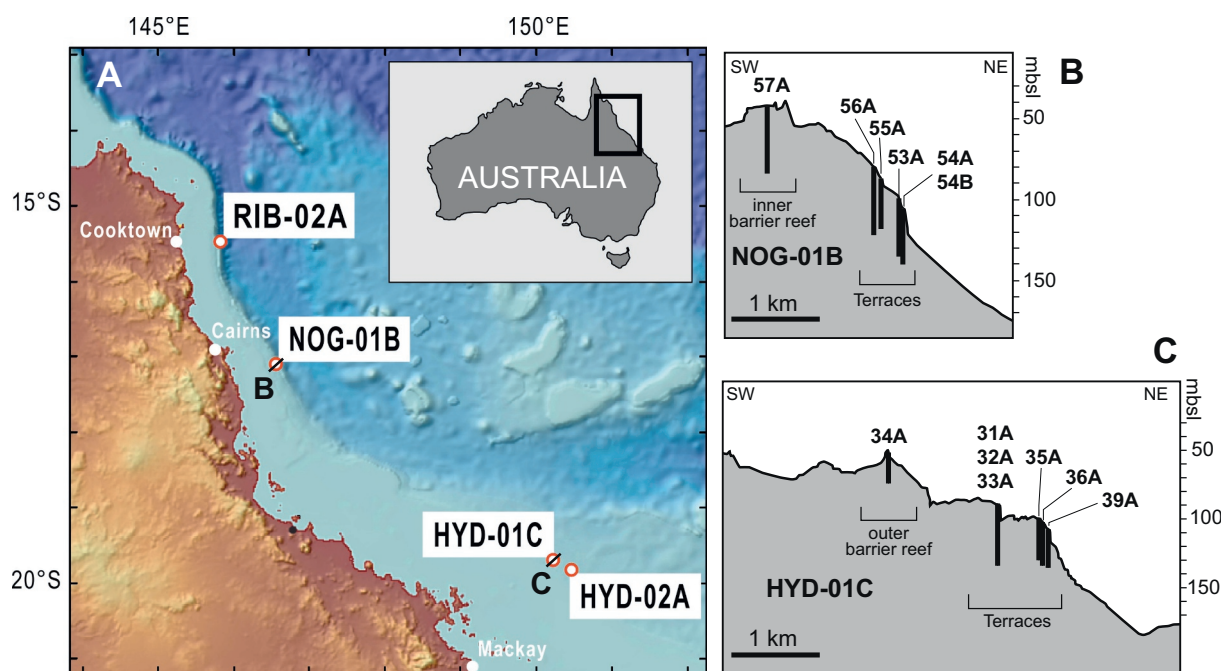

Fig. 1. A. Locations of drilling sites in the NE Australian shelf. B. Shelf edge profile and location of drilling holes at the Noggin Pass transect NOG-01B (see Fig. 3). C. Shelf edge profile and location of drilling holes at the Hydrographer's Passage transect HYD-01C (see Fig. 2).
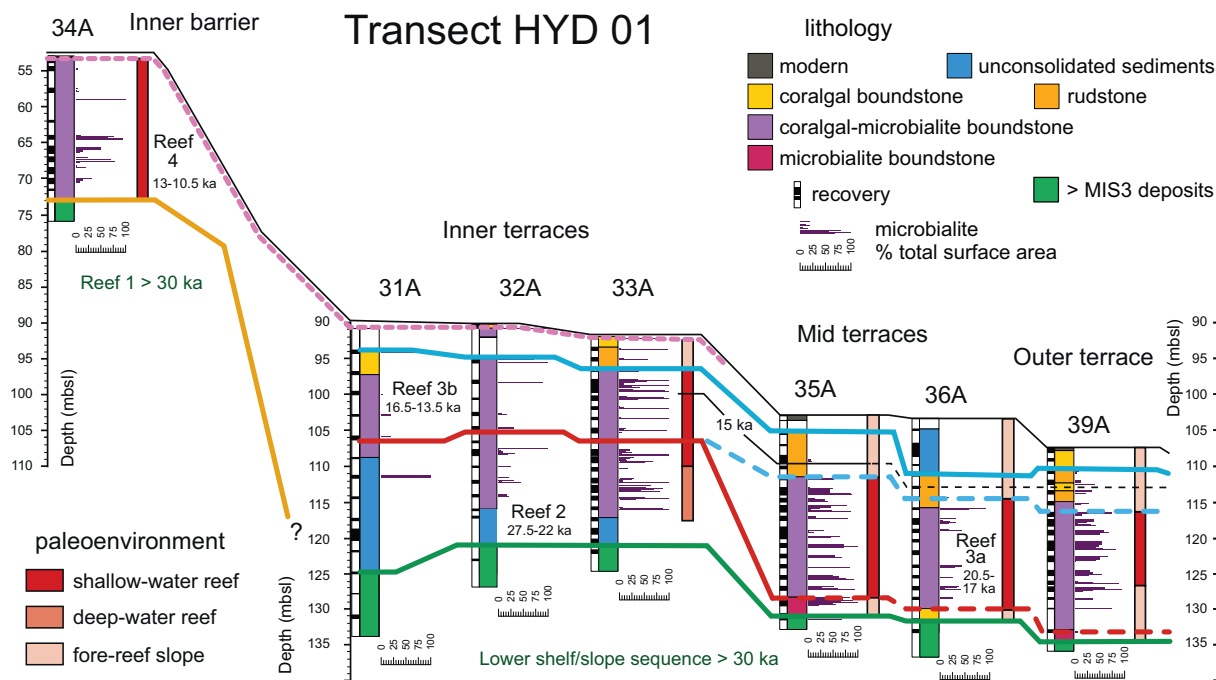(Modified after Webster et al., 2018).

Fig. 2. Hydrographer's Passage transect HYD-01C. Stratigraphic cross-section showing distribution of the main lithologies and facies, and percentage of microbialite cover on half-core surface. Paleoenvironmental interpretation after Webster et al. (2018) and Humblet et al. (submitted). Chronostratigraphic boundaries of reefs 1 to 4 are represented by the solid and dashed colored lines.

Fig. 3. Noggin Pass transect NOG-01B. Stratigraphic cross-section showing distribution of the main lithologies and facies, and percentage of microbialite cover on half-core surface. Paleoenvironmental interpretation after Webster et al. (2018) and Humblet et al. (submitted). Chronostratigraphic boundaries of reefs 1 to 4 are represented by the solid and dashed colored lines.
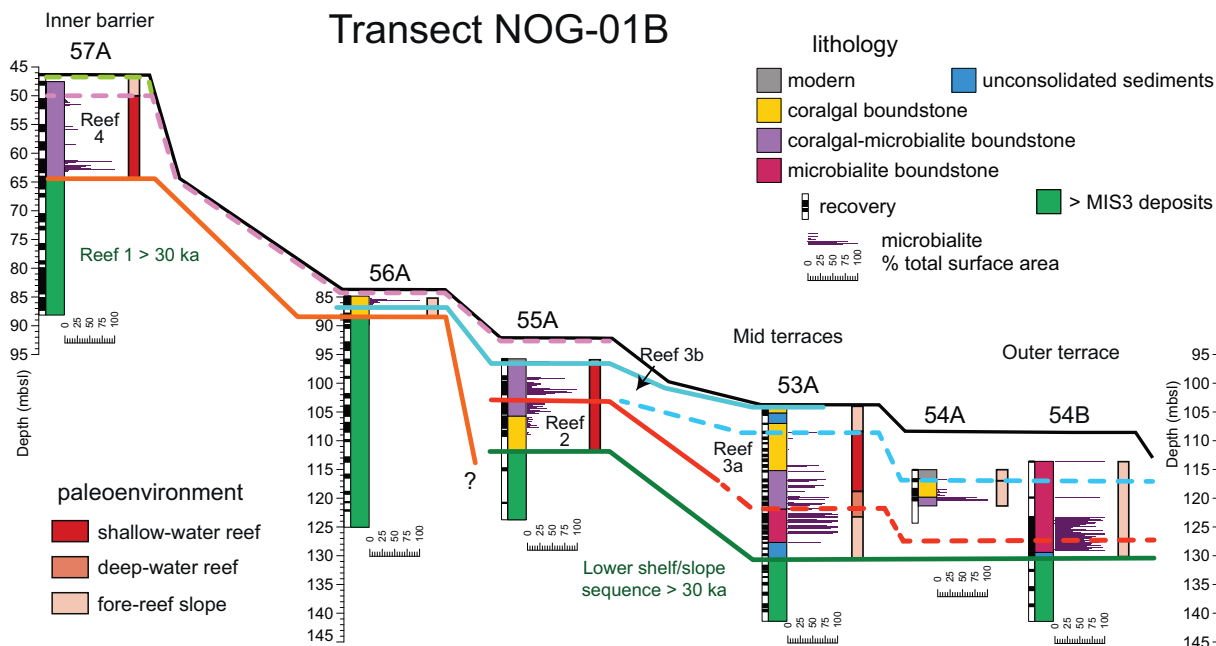
Cairns (Figs. 2 and 3). At HYD-01C, 11 reef sites with core recoveries ranging from 4 to 41% were drilled, and 10 reef sites with core recoveries of 1.4–42% at NOG-01B. Additionally, we examined cores and samples from hole M0040A, drilled on the outer terrace at transect HYD-02A off Mackay (Fig. 1).

2.2. Sampling and analytical techniques

Basic core logging was undertaken by the IODP Expedition 325 scientists (Webster et al., 2011). Specific logging of microbialites was carried out by a combination of visual examination of high-resolution digital line-scan images of the archive core halves, hand samples of slabbed core material, and petrographic thin sections. Microbialite proportion was measured as the percentage of microbialite fabric in the surface area of each core piece. Small pieces of microbialite were examined under a FEI Quanta-400 ESEM. Polished sections coated by evaporated carbon were used to distinguish carbonate types and to obtain their relative elemental composition at selected points. The

compositional images were obtained by a Solid State Back-scattered Detector and point microanalyses were made with an EDAX Sapphire Si (Li) energy dispersive detector with SUTW. The microanalyses have an accuracy of about Å ± 2%, using oxide and carbonate standards corrected for the geometry and settings of the microscope (Table S1). The analyses were made at 20 kV acceleration voltage at a working distance of 10 mm. Siliciclastic contents were estimated by determining the total carbonate content with a CM5240 Total Inorganic 207 Carbon autoanalyzer in 54 microbialite samples (Table S2). The 35 samples for C and O stable isotope analysis were collected from microbialite lacking visible bioclasts. All samples were cleaned with an ultrasonic cleaner and washed in demineralized water and dried at 40° C. Analyses were carried out in the Centro de Instrumentación Científica of the Universidad de Granada using an Isoprime Dual Inlet Mass Spectrometer with Multiprep and Gilson autosampler (Table S3). Carbonate samples were reacted with 103% phosphoric acid at 90 °C during 10 min. Results are reported relative to V-PDB calibrated with replicate analysis of the NBS-19 values. The external reproducibility of both isotopic measurements was < 0.05‰, obtained by replicate analysis of an internal carbonate (marble) standard with values of −3.38‰ and 2.47‰ for $\delta^{18}O$ and $\delta^{13}C$, respectively.

Four microbialite samples of different facies types from the NOG-01B transect (Table S4) were analyzed for lipid biomarker contents. The detailed decalcification and extraction protocols can be found in Heindel et al. (2010). After saponification of the total lipid extract (TLE) with 6% KOH in methanol, the samples were extracted with a microwave extraction system (CEM Discovery) at 80 °C and 250 W with a dichloromethane:methanol (3:1) mixture. The total extracts were separated into *n*-hexane soluble (maltenes) and dichloromethane-soluble (asphaltenes) fractions. The *n*-hexane fraction was further separated by column chromatography into four fractions of increasing polarity (cf. Birgel et al., 2008). The interpretations are based on the alcohol and fatty acid fractions, which contained source-specific biomarkers. The hydrocarbon and ketone fractions are not discussed further due to the absence of source-specific patterns.

Both alcohols and fatty acids were analyzed by coupled gas chromatography–mass spectrometry (GC–MS) with an Agilent 7890 A GC system coupled to an Agilent 5975 C inert MSD mass spectrometer at the Department of Geodynamics and Sedimentology, University of Vienna. Compounds were quantified by gas chromatography-flame ionization detection (GC-FID) with an Agilent 7820 A GC system. Both GC–MS and GC-FID were equipped with a 30 m HP-5 MS UI fused silica capillary column (0.25 mm i.d., 0.25 μm film thickness). The carrier gas was helium. The GC temperature program used was as follows: 60 °C (1 min); from 60 °C to 150 °C at 15 °C/min; from 150 °C to 320°C at 4 °C/min. The final temperature was held for 37 min. Identification of compounds was based on retention times and published mass spectra. For better comparability of the various samples with different biomarker contents, all quantified fatty acids and alcohols are displayed as wt%, the relative quantities are expressed in ng/g (= ng lipids/g rock):

Specified biomarker (wt%) = (Specified biomarker (ng·g⁻¹)·

$$\text{(sum of all compounds (ng·g}^{-1}))^{-1}\cdot100\%$$

$$(1)$$

Compound-specific carbon isotope analysis was performed with a Thermo Fisher Trace GC Ultra connected via a Thermo Fisher GC Isolink interface to a Thermo Fisher Delta V Advantage spectrometer at the Department of Terrestrial Ecosystem Research, University of Vienna. Conditions chosen for gas chromatography were identical to those described above. Carbon isotopes are given as δ values per mil relative to the V-PDB standard. Each measurement was calibrated using several pulses of carbon dioxide with known isotopic composition at the beginning and end of the run. Instrument precision was checked with a mixture of *n*-alkanes (C_{14} to C_{38}) of known isotopic composition. Analytical standard deviation was < 0.5‰.

3. Geological and stratigraphic setting

3.1. Structure and composition of the shelf edge reefs

The cored reef deposits on the GBR shelf edge comprise two basic sequences, separated by a major unconformity surface: 1) basal > MIS3 (~30 ka) deposits, and 2) overlying MIS2 to last deglacial deposits (Webster et al., 2011, 2018; Hinestrosa et al., 2014; Yokoyama et al., 2018) (Figs. 2 and 3). Here we concentrate on the microbialites of the younger sequence (sequence 2).

The MIS2 to deglacial coral reef deposits are mainly composed of boundstone and detrital sediments. Three boundstone facies were defined based on their proportions of coral, crustose coralline algae (CCA) and microbialite: coralgal boundstone, coralgal-microbialite boundstone and microbialite boundstone (< 25% of coralgal framework) (Webster et al., 2018; Humblet et al., submitted). In the coralgal framework, corals are commonly veneered by centimeter-scale coralline algal crusts, associated with vermetid gastropods and encrusting foraminifers. The detrital consolidated and unconsolidated sediments (mud to gravel) are mainly composed of mollusks, bryozoans, echinoids, benthic foraminifers, red algae and *Halimeda*. They occur as internal sediment in boundstones, or as 1–19 m thick intervals either beneath the boundstone facies (holes M0053, 31–33A) or intercalated within them (hole M0036A).

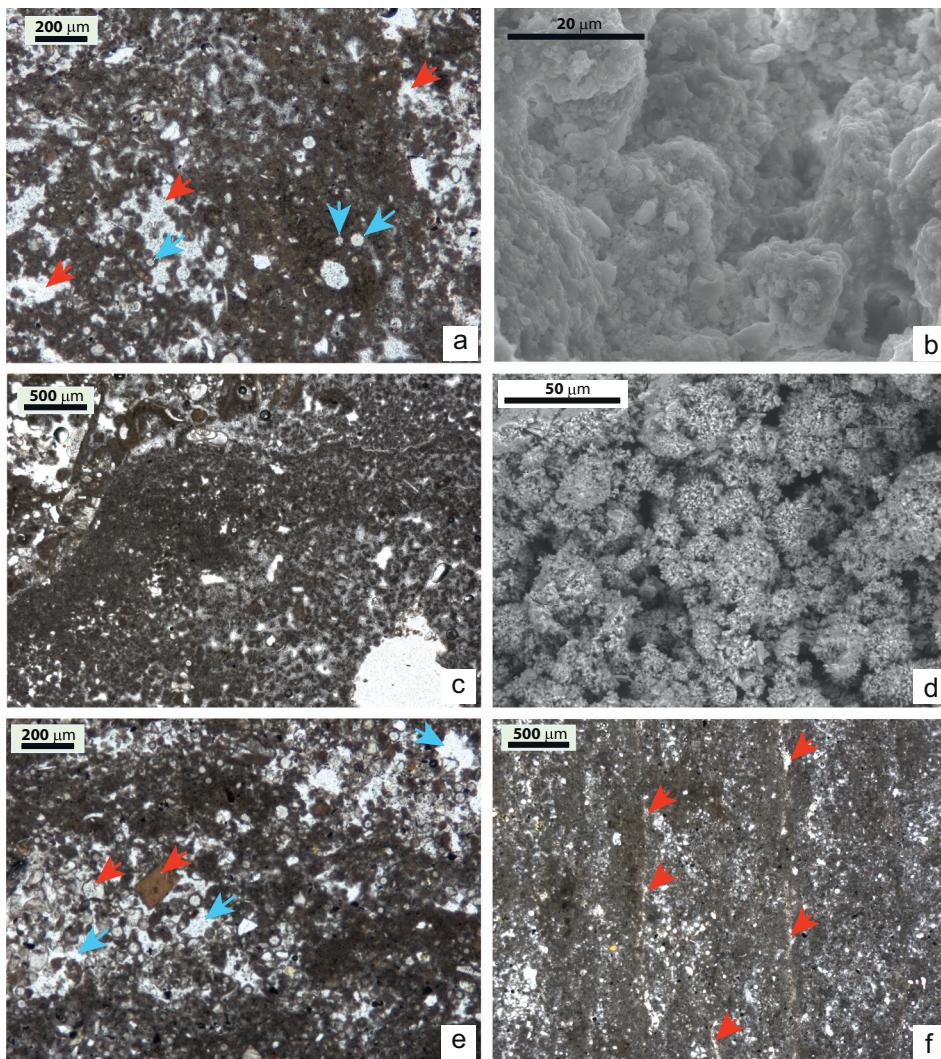### 3.2. Reef stacking patterns in the Great Barrier Reef from 28to 10 ka

Detailed chronological analyses based on U-series and ¹⁴C-AMS dating of > 580 corals and coralline algae show complex stacking of a series of reef phases in the GBR over the last 30 ka. Four distinct reefs that grew from 28 to 27 to 10 ka display offlapping and backstepping patterns in response to sea-level fall followed by progressive sea-level rise (Yokoyama et al., 2018; Webster et al., 2018) (Figs. 2 and 3). Reef 2, according to the nomenclature of Webster et al. (2018), began to grow at 27.5 ka, after the global sea-level fall from MIS3 to MIS2. Following a short period of accretion, growth stopped at 22 ka as sea level fell to its lowest LGM level and shallow reefs migrated basinward. Reef 3a grew on top of the fore-reef deposits of Reef 2 from 20.5 to 17 ka. Sea-level rise during deglaciation resulted first in aggradation of Reef 3a, and then in retrogradation and onlapping of the top of Reef 2 by 16.5 ka. Continued sea-level rise led to development and accretion of Reef 3b until it was drowned at 13.5 ka. Subsequently, shallow-water corals backstepped onto basement older than 30 ka. During the last deglacial phase, Reef 4 aggraded in the inner barrier from 13 to 10.5 ka (Yokoyama et al., 2018; Webster et al., 2018) (Figs. 2 and 3). Coralgal assemblages (Webster et al., 2018; Humblet et al., submitted) and chronostratigraphic patterns (isochrons) within each reef phase allow precise paleo-depth reconstructions of coralgal-microbialite and microbialite boundstones within high-resolution time slices (Figs. 2 and 3).

4. Results

4.1. Microbialite components

The microbialite consists of differing proportions of micrite/microspar, allochthonous grains (bioclastic and siliciclastic), fenestrae and encrusting epibionts.

Micrite/microspar form the matrix of the microbialite. They range from clotted to homogeneous, with density reflected by the degree of darkness under the optical microscope (Fig. 4a). Clotted microfabrics comprise irregular dark areas surrounded by irregular lighter ones, with transitions from micrite to microspar, and irregular fenestrae (Fig. 4a). Under the ESEM, clotted micrite consists of irregularly shaped aggregates of small blocky crystals of high-magnesian calcite, surrounded by irregular, smaller empty spaces. Crystal size ranges < 1 μm to 10 μm (Fig. 4b).

Fig. 4. Microbialite microfabrics. a) Clotted micrite/microspar microfabrics showing irregular dark areas surrounded by irregular lighter ones with transitions from micrite to microspar, and irregular voids (fenestrae, red arrows). Changes in darkness reflect changing density. Blue arrows point to ascidian spicules. Sample 54B.8.1.2.12. b) ESEM view of clotted micrite. Irregularly shaped aggregates of small blocky crystals of high-magnesian calcite are surrounded by empty spaces. Crystal size is < 10 μm. Sample 39A.15.1.25–28. c) Peloidal microfabric (bottom right) changing to clotted micrite/microspar rich in bioclasts (top left). Dense calcite aggregates (peloids), 20 to 40 μm in diameter, radially transition to microspar that lines the empty voids between them. Sample 54B.7.1.62–70. d) ESEM view of peloidal microfabric. Peloids consist of a nucleus of small crystals (about 1 μm or less in size) surrounded by rhombohedral crystals, up to 10 μm in size. Sample 39A.15.1.25–28. e) Grainstone, packstone and wackestone microfabrics. Bioclasts (locally with siliciclastic grains, red arrows) can form grain-supported microfabrics (packstone, grainstone, rudstone) according to micrite content and grain size. The transitions between different microfabrics are abrupt at thin-section scale. Blue arrows indicate fenestrae of different size and shape. Sample 54B.7.1.62–70. f) Small bioclasts dispersed within micrite. The microfabrics resemble mudstone, wackestone or floatstone, depending on grain abundance and size, although in situ microbial origin of the micrite would imply that the fabric is a boundstone. Flat fenestrae (red arrows) outline lamination. Sample 54B.7.1.96–99. (For interpretation of the references to color in this figure legend, the reader is referred to the web version of this article.)

Peloidal microfabric is a distinctive variety of the micrite/microspar component, made up of a frame of boudin-like calcite aggregates, 20 to 40 μm in diameter, separated by smaller empty spaces. Under the optical microscope the internal structure is seen as a dense micrite nucleus radially transitioning to microspar that lines the empty voids between the peloids (Fig. 4c). Under the ESEM, each peloid consists of a mass of small crystals (about 1 μm or less in size) surrounded by more or less radially arranged rhombohedral crystals, up to 10 μm in size, producing a druse-like surface (Fig. 4d).

Micrite in homogeneous, clotted and peloidal microfabrics, is made up of high-magnesian calcite, with 10 to 15 mol% MgCO$_3$ (Table S1).

Most allochthonous particles are bioclasts, but quartz grains occur locally. Bioclasts locally form densely packed grain-supported microfabrics that can be described as packstone, grainstone (Fig. 4e) and rudstone, according to grain size and the proportion of micrite. Commonly, however, grains are dispersed within micrite and the microfabric corresponds to mudstone, wackestone (Fig. 4f) or floatstone. However, since the micritic matrix is most likely biogenically induced, the facies as a whole could be described as boundstone. Recognizable bioclasts include corals, alcyonarian spicules, bryozoans, serpulids, vermetids and other mollusks, echinoids, *Halimeda*, coralline algae and benthic and planktonic foraminifers. Ascidian spicules are very common and locally are the only identifiable component in fine-grained microfabrics (Fig. 5a, also arrows in Fig. 4a). Bioclast size ranges from

micrometers to several centimeters (Figs. 5b and 6). Silt-sized bioclasts can be identified as particles brighter (higher atomic weight areas) than the microbial micrite groundmass in backscattered electron images, and by Sr content in aragonitic grains (Fig. 5b). The siliciclastic content is 7.5% on average and can locally reach 14.5% (Table S2); quartz grains are visible in many core intervals.

In situ encrusting epibionts are common. Encrusting foraminifers, solitary individuals or clusters of vermetids, bryozoans, serpulids, and, locally, thin CCA attached to microbialite accretion surfaces and were buried by continued microbialite growth (Figs. 7a, b & 8a).

Fenestrae show large variations in shape, size and orientation (Fig. 4a, e and f), and usually have angular contours that range from sharply defined to transitional to clotted micrite/microspar. Locally they have 'stromatactis' shape. Their sizes range from micrometers to millimeters. Fenestrae can be empty, partially to completely filled with microbial packstone to grainstone, or lined to completely filled by cement.

The δ^{13}C values of microbialite bulk carbonate samples from the Noggin area range from 2.6 to 5.6‰ (average 3.9‰, std. 0.7), and δ^{18}O values are between −0.4 and 1.2‰ (average 0.7, std. 0.4) (Table S3). The δ^{13}C values in microbialite bulk carbonate samples from the Hydrographer's area range from 3.1 to 4.3‰ (average 3.9‰, std. 0.3) and δ^{18}O values are between 0.5 and 1.2‰ (average 1.0‰, std. 0.1, Table S3). The δ^{13}C and δ^{18}O values of microbialite bulk carbonate
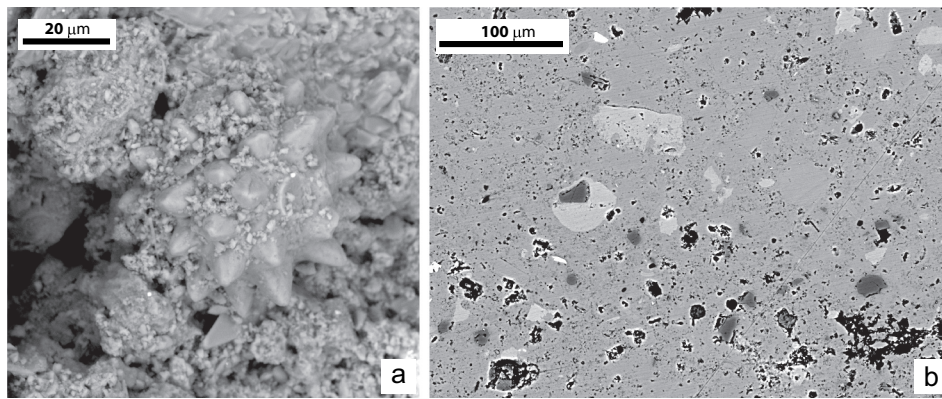
Fig. 5. Microbialite bioclastic components. a) ESEM view of an ascidian spicule within micrite matrix. Sample 53A.20.1.5–10. b) Silt-sized bioclasts are common in GBR microbialite (particles brighter - higher atomic weight areas - than the microbial micrite groundmass in backscattered electron images). Sample 54B. 6.1.84–95.

Fig. 6. Microbialite coated debris (MCD fabric). Coral fragments (blue arrows), *Halimeda* segments (red arrows), bivalve shells (green arrow) coated by microbialite (arrowheads). Note borings in both microbialite and bioclasts. Sample 39A 4.1.26–36. (For interpretation of the references to color in this figure legend, the reader is referred to the web version of this article.)

samples from Reef 2 in both areas have average values of 4.0‰ (std. 0.1) and 0.9‰ (std. 0.1), respectively (Table S3, Fig. 9). Samples from Reef 3a yielded similar values (average $\delta^{13}C$ = 4.0‰, std. 0.4; average $\delta^{18}O$ = 0.9‰, std. 0.2). The values from Reef 3b bulk carbonate samples are lower (average $\delta^{13}C$ = 3.3‰, std. 0.4; average $\delta^{18}O$ = 0.4‰, std. 0.3) (Table S3, Fig. 9). Samples altered by soil processes during LGM emersion of Reef 2 show significantly lower $\delta^{13}C$ and $\delta^{18}O$ values (1.5 to 2.3‰ and −1.5 to 0.0‰, respectively, Table S3).

4.2. Microbialite fabrics

Microbialite components typically appear combined in five basic mesoscale fabrics that are recognizable in visual core examination: laminated microbialite, structureless microbialite, digitate microbialite, microbialite-coated debris, and intraskeletal and boring-filling microbialite (Fig. 8a–d).
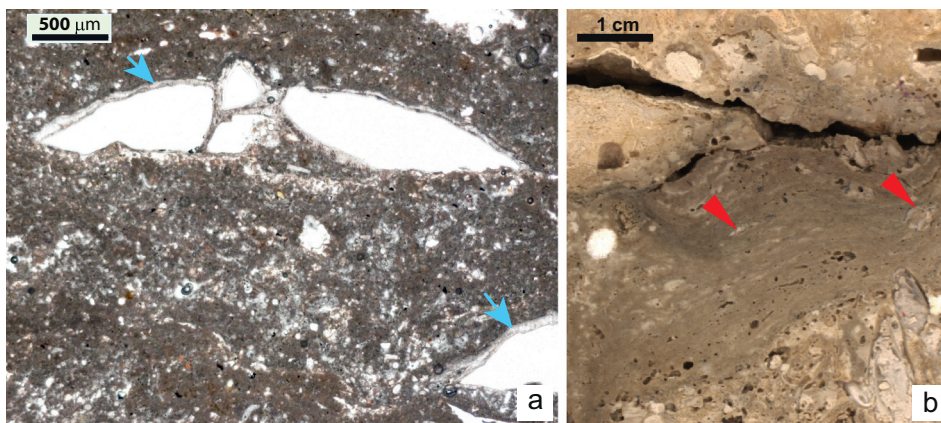
Laminated microbialite (LM) is a stromatolitic fabric, well-known in microbial deposits. This is the most common fabric in LGM and postglacial microbialites observed by us in the GBR. The lamination can be diffuse to distinct, changing within a few centimeters in the same crust. Laminae (< 3 mm) show a wide variation in thickness and can have short lateral continuity. They can be concentric and parallel to their substrate, form small domes (Fig. 8a), or define internal digitations. Internal unconformities between lamina sets are common (Fig. 7b). Lamination is produced by changes in micrite microfabric and density, changes in grain packing and size (Fig. 4f), fenestra shape and orientation, and, locally, orientation of encrusting epibionts. Flat parallel fenestrae locally help to outline lamination (Fig. 4f).

Structureless microbialite (SM) comprises crusts of microbialite with no distinct internal pattern (Fig. 8b). Under the microscope it consists of irregular patchy areas of varying size, from hundreds of micrometers to millimeters, with varied micrite/microspar content and density, variations in grain packing and size, and different proportions, size and shape of fenestrae. Encrusters are common, and this fabric also usually has a high content of large bioclasts.

Digitate microbialite (DM) is arranged in knobby, rarely branching protuberances, several millimeters in diameter and usually < 1 cm high (Fig. 8b). Internally it can be similar to the structureless fabric or show diffuse lamination. It is relatively rare in LGM and postglacial microbialites in the GBR.

Microbialite-coated debris (MCD) consists of matrix- to grain-supported bioclastic breccia with large bioclasts (up to several centimeters) surrounded by microbial carbonate (Fig. 6). Corals, CCA (including small rhodoliths), mollusks, echinoids, foraminifers and *Halimeda* are common bioclasts. Under the microscope, the fabric comprises irregular patches, some with sharp edges, with varying proportions of micrite microfabric, diverse grain packing and size, and fenestrae of diverse shape and size. Some patches show internal lamination, and peloidal microfabric is common. Some microbialite patches fill borings, and locally create geopetal structures. Platy to platy-digitate encrusting corals within the breccia appear to be in life position, and encrusting epibionts are common on microbialite accretion surfaces.

Intraskeletal and boring-filling microbialite (IBFM) partially or totally infills primary voids and cavities generated by bioeroders in invertebrate and calcareous algal skeletons (Fig. 8a and b). Microbialite that formed in spaces between thalli in frameworks of contorted foliose CCA can also be included in this category. The infilling microbial
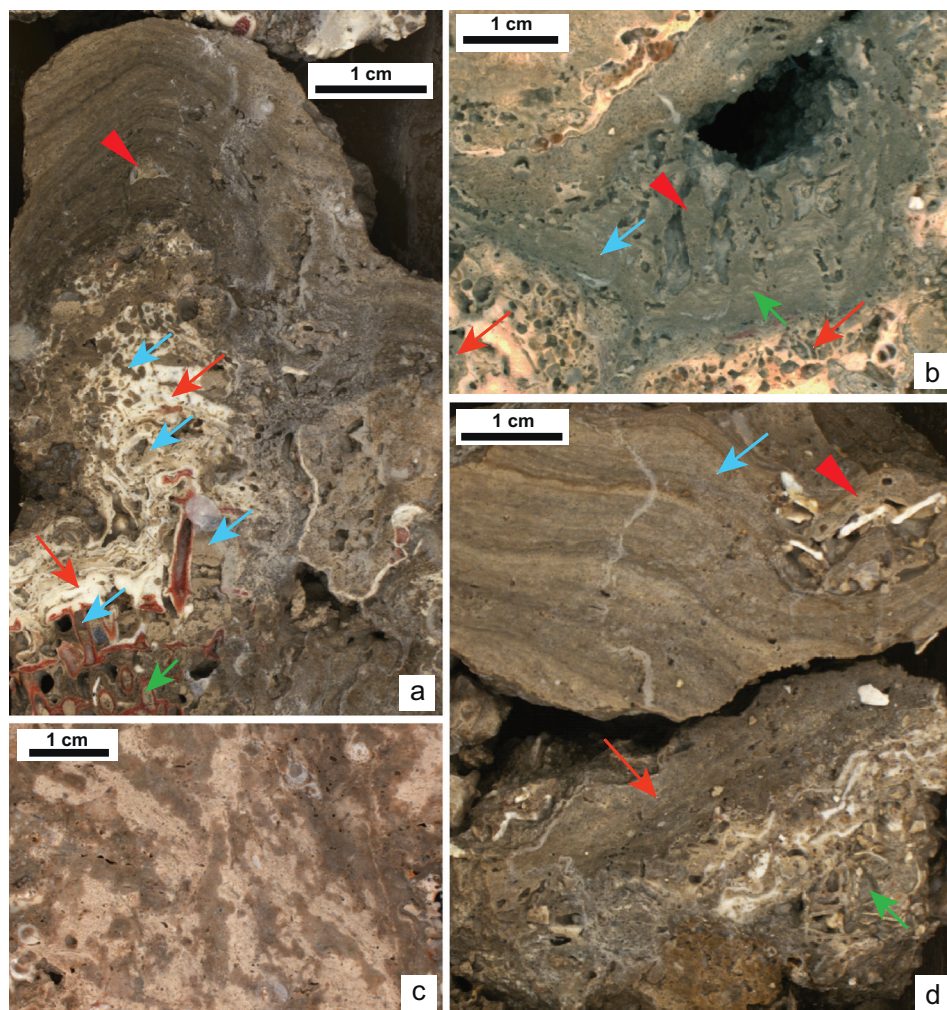
Fig. 7. Encrusters. a) Vermetids (arrows) growing on microbialite accretion surfaces. Sample 54B.7.1.96–99. b) Vermetids (arrowheads) intergrown with laminated microbialite. Sample 33A 5.1.113–118.

carbonate shows diverse proportions of micrite microfabric, from homogeneous to peloidal, and varied grain packing and size. The microbialite filling the voids can be similar to that which grows on the same skeleton, or may only consist of peloidal micrite. Commonly, however, an initial fill-phase of 'packstone-wackestone' microbialite is followed by peloidal micrite and/or fine-grained grainstone. These successions can produce a very delicate lamination. Several phases of boring/microbialite filling are locally present. This type of microbialite

penetrates the outer millimeters to few centimeters of skeletal framebuilders and larger bioclasts, and usually grades into other overlying fabrics (Fig. 8a).

All microbialite samples studied show borings with a wide range of size and shape. Borings range in size from hundreds of micrometers to centimeters, and can have individually well-defined shapes, such as *Gastrochaenolites*, or form complex networks of irregularly varying shapes (Figs. 7b, 8a and b).

Fig. 8. Microbialite mesoscale fabrics. a) Intraskeletal and boring-filling microbialite (blue arrows) in coralline algal crusts (red arrows) and in the octocoral *Tubipora* (green arrow), all covered by a small dome of laminated microbialite. Note vermetid (arrowhead) growing on an accretion surface of the laminated microbialite. Sample 54B 6.1.66–75. b) Intraskeletal and boring-filling microbialite (red arrows) in corals and coralline algal crusts covered by structureless microbialite (blue arrow), laminated microbialite (green arrow) and digitate microbialite (arrowhead) on top. Sample 33A 5.1.100–105. c) Microbialite altered by soil processes. Sample 55A 4.2.1.113–118. d) Microbialite coated debris (green arrow) overlain by structureless microbialite (red arrow), and microbialite coated debris (arrowhead) overlying laminated microbialite (blue arrow) at the top. Sample 53A 20.1.23–29. (For interpretation of the references to color in this figure legend, the reader is referred to the web version of this article.)
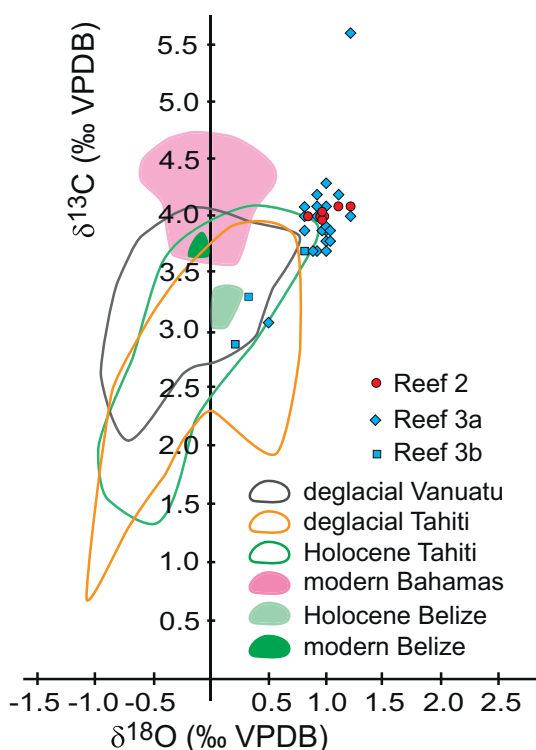
Fig. 9. δ^{13}C and δ^{18}O values of microbialite bulk carbonate samples from Reefs 2, 3a, and 3b from both Noggin and Hydrographer's transects. Contour lines and colored areas envelop δ^{13}C and δ^{18}O values of microbialite samples from Tahiti (mainly Holocene samples, Camoin et al., 1999; deglacial, Heindel et al., 2010), Vanuatu (Cabioch et al., 2006), Bahamas (modern, Andres et al., 2006) and Belize (Holocene micrite crust, Gischler et al., 2017a; modern cave biostalactites, Gischler et al., 2017b).

4.3. Microbialite-fabric distribution in LGM and deglacial GBR reefs

The distribution of microbialite fabrics in the different facies building the LGM and deglacial reefs is detailed in Tables 1 and 2, respectively (see also Fig. 10). Microbialite at the top of Reef 2 in hole M0055A is diagenetically altered (Fig. 8c). The stratigraphy and assignation of core intervals to successive reefs phases follows Webster et al. (2018).

4.4. Lipid biomarker inventory

4.4.1. Hydrocarbons

Most common compounds in microbialites from all sites in the hydrocarbon fractions are *n*-alkanes with chain lengths ranging from n-C_{16} to n-C_{33} (not shown). Because contents are low and diagnostic compounds are lacking, this fraction is not described in more detail.

4.4.2. Alcohols

In microbialites GBR 1 to 4, long-chain *n*-alcohols with carbon chains from C_{25} to C_{28} and contents ranging from 1 to 2 wt% were found (see Eq. (1) in Section 2.2). Long-chain *n*-alcohols derive from leaf waxes of higher land plants (e.g., Eglinton and Hamilton, 1967). Non-isoprenoidal *sn*-1-mono-*O*-alkyl glycerol ethers (MAGEs) with *n*-alkyl chains ranging from C_{14} to C_{18} (Fig. 11) occur in all GBR samples, representing contents from 1 wt% in GBR 2 and 3 to 2 wt% in GBR 4 (Tables 3 and 4). These ether compounds have only been recognized in few cultured, mostly thermophilic, bacteria, including sulfate-reducing bacteria (Langworthy et al., 1983; Rütters et al., 2001; Grossi et al., 2015; Vinçon-Laugier et al., 2016, 2017, 2018).

The sterols brassicasterol, dinosterol, gorgosterol, stigmasterol, campesterol and β-sitosterol, as well as two other non-steroid cyclic

triterpenoids (germanicol and lupeol), were detected in all microbialites with higher contents than the long-chain alcohols. The most abundant sterols in all samples are β-sitosterol and gorgosterol. Combined abundances for brassicasterol, dinosterol and gorgosterol range between 1 wt% in GBR 3 and 4 wt% in GBR 2 and 4, while the combined abundances of the other cyclic triterpenoids, including germanicol and lupeol, range from 2 wt% in GBR 3 to 6 wt% in GBR 2 and 4 (Table 4). Brassicasterol is mostly synthesized by diatoms and other marine microphytoplankton, but may occur in higher plants as well (Volkman et al., 1989). Dinosterol indicates input of marine phytoplankton and is mainly produced by dinoflagellates and some diatoms (Boon et al., 1979; Volkman et al., 1993; Moldowan and Jacobson, 2000). Gorgosterol is an indicator for marine phytoplankton but is also a constituent of marine invertebrates, since it has been found not only in autotrophic dinoflagellates and some diatoms but also in symbiotic dinoflagellates (zooxanthellae) isolated from invertebrates (cf. Rampen et al., 2009 and references therein). Campesterol, stigmasterol, β-sitosterol, germanicol and lupeol are commonly interpreted to represent terrestrial biomarkers, since they derive from higher land plants, although marine algal sources cannot be excluded (Volkman, 1986). In particular, β-sitosterol, germanicol and lupeol may indicate input from mangroves (Volkman, 1986; Koch et al., 2011). The contents of the unspecific bacterial biomarker 17β(H),21β(H)-32-hopan-*ol* (bishomohopanol) range from 1 wt% in GBR 3 to 3 wt% in GBR 2 and 4.

4.4.3. Fatty acids

The contents of short-chain *n*-fatty acids (C_{14} to C_{19}, Fig. 11) range from 24 wt% in GBR2 to 31 wt% in GBR 3 and 4 (Table 4). In all samples, the saturated n-C_{16} fatty acid is the most abundant. High contents were found for the monounsaturated fatty acids $C_{16:1\omega7}$, $C_{18:1\omega7}$ and $C_{18:1\omega9}$ (9 to 13 wt%, Table 4), with $C_{18:1\omega9}$ fatty acid being most abundant. All detected saturated and unsaturated short-chain fatty acids are of low to moderate specificity and are found in marine bacteria (e.g., Parkes and Taylor, 1983), marine phytoplankton (e.g., Volkman et al., 1989), as well as zooplankton and marine benthos (e.g., Albers et al., 1996; Graeve et al., 1997).

Terminally branched *iso*- and *anteiso*-fatty acids with carbon chains ranging from C_{15} to C_{18} yielded contents from 5 wt% in GBR 3 to 8 wt% in GBR 4 (Fig. 11). Among these, *iso*- and *anteiso*-C_{15} and *iso*- and *anteiso*-C_{17} fatty acids are most abundant, with *iso*-fatty acids being more abundant than their *anteiso* counterparts. The mid-chain branched 10Me-$C_{16:0}$-fatty acid is less abundant, yielding contents of only 1 wt% in all GBR microbialites (Table 3). Short-chain branched fatty acids are constituents of various bacteria (e.g., Romano et al., 2008), but 10Me-$C_{16:0}$-fatty acids and *iso*- and *anteiso*-$C_{15:0}$ and $C_{17:0}$ fatty acids are particularly common in sulfate-reducing bacteria (e.g., Taylor and Parkes, 1983; Edlund et al., 1985; Kaneda, 1991; Elvert et al., 2003).

Long-chain *n*-fatty acids with carbon chains from C_{25} to C_{33} were found (Fig. 11) and correspond to 6 wt% in GBR 4, 7 wt% in GBR 2, and 13 wt% in GBR 3 (Tables 3 and 4); even-numbered carbon chains predominate over their uneven-numbered counterparts. They derive from leaf waxes of higher land plants, tracing terrestrial input (e.g., Eglinton et al., 1968).

Hopanoic acids are also present in all microbialites with abundances ranging between 4 wt% in GBR 2 and 3 and 6 wt% in GBR 4. Both, biological 17β(H), 21β(H) (ββ) and geological 17α(H), 21β(H) (αβ) configurations are present, including ββ-C_{32}, αβ-C_{33} and ββ-C_{33} hopanoic acids.

4.5. Carbon isotopic composition of lipid biomarkers

Short-chain *n*-fatty acids and most sterols from marine eukaryotes yielded average compound-specific δ^{13}C values of $-25‰$ (GBR 2) and $-24‰$ (GBR 3 and 4, Table 4). Terrestrial-derived biomarkers such as long-chain *n*-fatty acids and *n*-alcohols, germanicol, lupeol and other cyclic triterpenoids show a larger spread of δ^{13}C values ($-25‰$ in GBR
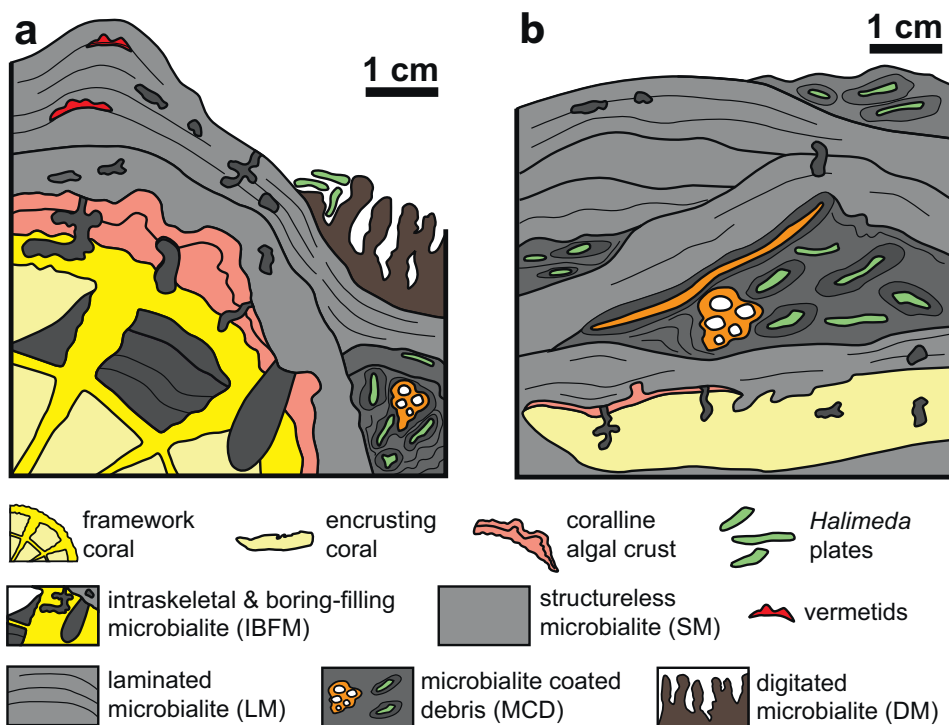
Table 1

Microbialite facies distribution in LGM reefs (Reefs 2 and 3a) in the GBR. IBFM: Intraskeletal and boring filling microbialite; SM: structureless microbialite; LM: laminated microbialite; DM: digitate microbialite; MCD: microbialite coated debris. bdst.: boundstone.

	Core interval	Facies	Microbialite fabrics	Other
Reef 2				
Transect HYD-01C				
Inner terraces	M0032A 8.3 to 15.1 M0033A 11.1 - below 19 cm to 19.2	Coralgal-microbialite bdst.	IBFM in and on corals encrusted by CCA and foraminifers, covered by thin (< 1 cm) SM rich in bioclasts followed by a few centimeters of LM, locally DM at the top. Pockets of MCD on or intercalated within LM and SM or directly on corals and CCA.	Bioerosion. Relatively large (< 1 cm) voids with geopetal infillings
Mid terraces	M0035A 19.1 to 20.2	Microbialite bdst.	MCD overgrown by wavy and microdome LM crusts, several centimeters thick; locally DM at the top. Large coral pieces with IBFM coated with thin SM followed by LM.	All fabrics bioeroded.
Transect NOG-01B				
Inner terraces	M0055A 4.1 -below 34 cm to 7.1- top 11 cm	Coralgal-microbialite bdst.	IBFM in coral skeletons and CCA-vermetid crusts, SM among the tubes of Tubipora and thin coral branches. Thin SM crusts rich in bioclasts on framebuilders covered by LM and MCD. MCD occurs as centimeter-scale accumulations on any other microbialite fabrics or on corals and CCA, can be in turn coated by SM or LM crusts.	Altered by diagenetic processes. Bizarre color patterns do not correspond to microfabrics or primary components. Fissures and voids partially filled by a fine-grained dark sediment
Mid terraces	M0053A 18.1 to 23.1	Microbialite bdst. Encrusting corals	LM is the dominant fabric, followed by MCD. IBFM occurs in coral/CCA pieces, coated by thin SM, rich in large bioclasts, changing to wavy or microdome LM, several centimeters thick. Many pieces of microbialite do not show any coral/CCA substrate but they can be fragments detached during coring operations. MCD occurs in pockets on or within LM or any other fabric.	All fabrics show a certain degree of bioerosion. Quartz grains are common
Outer terraces	M0054B 7.1 below 70 cm to 9.1 top 69 cm	Microbialite bdst. Encrusting corals	IBFM in corals and CCA, coated by thin SM rich in bioclasts and encrusters or directly overlain by MCD. SM and MCD followed by wavy LM, locally intercalating MCD pockets, locally DM at the top. MCD increases downhole.	
Reef 3a				
Transect HYD-01C				
Mid terraces	M0035A 7.1 to 18.2 M0036A 10.1 to 18.2	Coralgal-microbialite bdst.	IBFM in frame builders. Thin SM rich in invertebrate encrusters on corals and CCA, and between tubes in Tubipora and fine branching corals. SM followed by thicker microdome LM (up to 8 cm), ending by thin DM in a few points. MCD is common in some intervals, directly lying on corals/CCA or overlying SM and LM. MCD accumulations can be encrusted by LM.	All fabrics bioeroded.
Transect NOG-01B				
Outer terraces	M0039A 7.1 to 21.1	Coralgal-microbialite bdst.	Same as above	All fabrics bioeroded.
Mid terraces	M0053A 4.1 to 9.2	Coralgal bdst.	IBFM and thin (< 1 cm) SM coating the framebuilders	All fabrics bioeroded.
	M0053A 10.1 to 17.2	Coralgal-microbialite bdst.	IBFM in corals and CCA crusts, covered by thin SM, rich in bioclasts and encrusters, followed by MCD and thin (< 5 cm) LM, locally forming microdomes. MCD and LM alternate in some points.	All fabrics bioeroded.
Outer terraces	M0054A 2.1 - below 25 cm to 3.1	Coralgal-microbialite bdst.	IBFM in corals and CCA and MCD around framebuilder pieces	All fabrics bioeroded.
	M0054A 4.1	Coralgal-microbialite bdst. Microbialite bdst. Corals are mainly encrusting *Porites*	Coralgal pieces, including IBFM, engulfed in MCD, thin (< 5 cm) SM and LM. IBFM in corals and CCA, coated by thin SM rich in bioclasts and encrusters or directly overlain by MCD. SM and MCD followed by thick wavy and microdome LM (up to 12 cm), locally intercalating MCD pockets, locally DM at the top.	All fabrics bioeroded. All fabrics bioeroded.
	M0054B 3.1 to 7.1 top 70 cm			

Table 2
Microbialite facies distribution in postglacial reefs (Reefs 3b and 4) in the GBR. IBFM: Intraskeletal and boring filling microbialite; SM: structureless microbialite; LM: laminated microbialite; DM: digitate microbialite; MCD: microbialite coated debris. bdst.: boundstone.

	Core interval	Facies	Microbialite fabrics	Other
Reef 3b				
Transect HYD-01C				
Inner terraces	M0032A 3.1 to 8.2 M0033A 2.1 below 14 cm to 11.1 top 19 cm	Coral-microbialite bdst. Coral-microbialite bdst. and rudstone	IBFM in the external sides of coral and CCA. Thin SM (< 1 cm) changes to microdome and wavy LM, up to 8 cm thick, locally with thin DM at the outer surface. MCD on framebuilders and on/within crusts. MCD increases uphole in M0033A cores.	All fabrics are intensively bored
Mid terraces	M0035A 3.1 to 6.2 M0036A 7.1 to 9.2	Rudstone	MCD and IBFM in larger coralgal pieces.	All fabrics bioeroded.
Outer terraces	M0039A 3.1 to 6.2	Rudstone and coralgal bdst.	IBFM in coralgal pieces. Thin (< 1 cm) SM, LM and DM on corals and CCA, followed by MCD overgrown by LM, several cm thick.	All fabrics bioeroded.
Transect NOG-01B				
Inner terraces	M0055A 2.1 to 4.1 top 34 cm M0056A 2.1 top 68 cm	Coralgal bdst.	IBFM in coral and CCA. Thin SM (< 4 cm) on frame builders, and MCD in framework spaces. LM and DM also on MCD pockets	All fabrics bioeroded.
Mid terraces	M0053A 1.1 to 3.1	Unconsolidated material		
Outer terraces	M0054A 2.1 to 2.1 top 25 cm M0054B 1.1	Rudstone	Pieces of MCD and LM	All fabrics bioeroded
Reef 4				
Transect HYD-01C				
Inner barrier	M0034A 1.1 below 24cm to 13.2	Coralgal-microbialite bdst.	IBFM in corals and CCA, MCD among corals, thin (< 5 cm) SM and LM on framebuilders and MCD pockets. Locally DM at the top	All fabrics bioeroded
Inner terraces	M0032A 1.1 to 1.2 M0033A 1.1 to 2.1 top 14 cm	Coralgal bdst.	IBFM in corals and CCA, MCD among corals, thin (< 5 cm) SM and LM.	All fabrics bioeroded
Mid terraces	M0036A 2.1 to 6.1	Rudstone and unconsolidated material	IBFM in larger coral pieces and MCD, locally followed by LM	All fabrics bioeroded
Outer terraces	M0039A 1.1 to 2.2	Coralgal bdst. and rudstone (top 37 cm)		
Transect NOG-01B				
Inner barrier	M0057A 2.1 to 7.1 top 38 cm	Coralgal-microbialite bdst.	IBFM in coralgal builders. Thin (< 2 cm) and scarce SM and LM on framebuilders. MCD within the framework.	All fabrics bioeroded
Inner terraces	M0056A 1.1 to 1.2	Rudstone. Encrusting corals	IBFM in larger coralgal pieces and MCD	All fabrics bioeroded

Fig. 10. a) Scheme of microbialite succession in coralgal-microbialite boundstone. Intraskeletal and boring-filling microbialite (IBFM) is the first fabric to develop. The framework skeletons and first phase of IBFM are overlain by structureless or laminated crusts with diffuse lamination. These crusts are usually overgrown by laminated microbialite that locally terminate in a veneer of digitate microbialite. Microbialite coated debris can appear at any stage of the succession, overlying the framework skeletons or intercalated within any of the other fabrics. As bioerosion continued during crust accretion, new generations of borings were opened and filled by IBFM. b) In microbialite boundstone, encrusting corals locally covered by coralline algal crusts and microbialite coated debris are covered by structureless and laminated crusts. Digitate microbialite is rare in this facies.

2 to −22‰ in GBR 3 and 4). Bacterial-derived compounds with low to moderate source specificity (*iso*-fatty acids C_{16} and C_{18}, hopanoic acids, bishomohopanol) show higher $\delta^{13}C$ values, from −21‰ in GBR 2 and 4 to −20‰ in GBR 3. Compounds interpreted to be sourced from sulfate-reducing bacteria, including MAGEs, 10Me-$C_{16:0}$-fatty acid and *iso/ anteiso*-$C_{15:0}$ and $C_{17:0}$ fatty acids, revealed the highest compound-specific $\delta^{13}C$ values, ranging on average between −19‰ in GBR 2 and 4 and −18‰ in GBR 3. Among them, the MAGEs yielded the highest $\delta^{13}C$ values (−17 to −16‰, see Tables 3 and 4).

5. Discussion

5.1. Composition
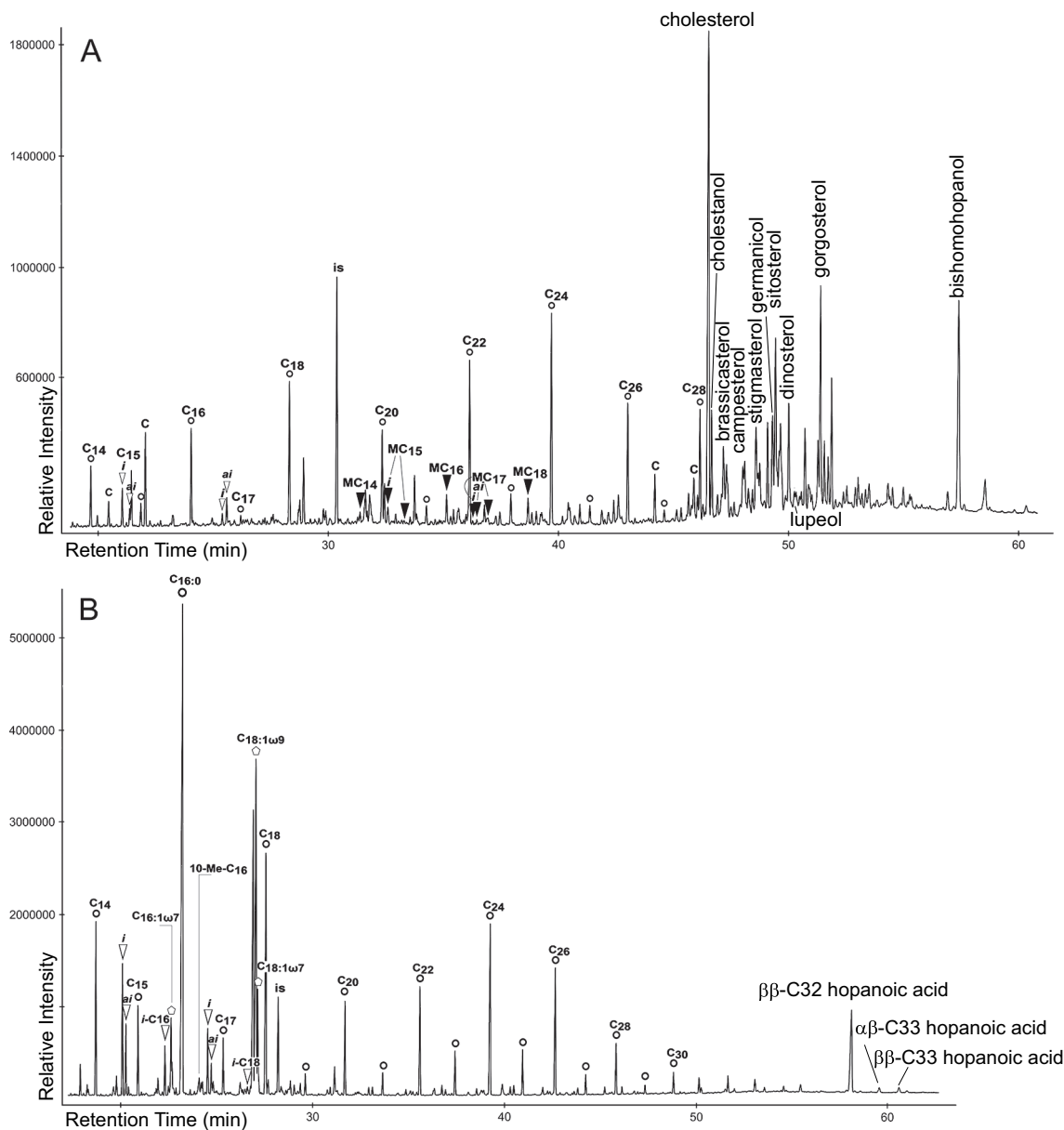
Typically, reefal microbial carbonate is high-magnesian calcite. Previously published contents show a range of 12–18 mol% $MgCO_3$ (Riding, 2011a and references therein) similar to the one obtained in the LGM and deglacial microbialites in the GBR. No variations in $MgCO_3$ content related to depth or other obvious environmental gradients have been observed (Camoin et al., 2006).

LGM and deglacial reef microbialites are generally rich in bioclasts, and this has been attributed to the adhesive EPS-rich surfaces of the former microbial mat (Camoin et al., 1999; Westphal et al., 2010). In the GBR microbialites there is a wide range of bioclast proportions in the different microfabrics. Large bioclasts are obviously main components of the MCD fabric, but they are also common in SM and LM fabrics. In all fabrics, sand-sized bioclasts are abundant and packstones and even grainstones fill voids in the IBFM, and form patches and laminae in the crusts. SEM examination reveals a high content of silt-sized bioclasts even in mudstone. Bioclasts are common in microbialites from deglacial reefs in Tahiti and the Marquesas (Camoin et al., 2006; Westphal et al., 2010; Seard et al., 2011), but are scarce in other Pacific last deglacial reefs, such as those in Vanuatu (Cabioch et al., 2006). However, even the largest previously reported percentage, up to 23% of aragonitic components (assumed to mainly represent bioclasts) in Tahiti (Seard et al., 2011), is low relative to the high bioclast content observed in the GBR, which can locally exceed 50% of the volume.

The stable oxygen and carbon isotope values of bulk carbonate from GBR microbialites (Table S3) are generally higher than those at Tahiti (Camoin et al., 1999; Heindel et al., 2010), Vanuatu (Cabioch et al., 2006) and Belize (Gischler et al., 2017a) (Fig. 9). The average values of the GBR microbialites ($\delta^{13}C$ 3.9‰, $\delta^{18}O$ 0.9‰) resemble the highest values of the Tahiti and Vanuatu microbialites. The high $\delta^{13}C$ values overlap the range of carbon isotopic composition of micrite crusts in Bahamian stromatolites, slightly ^{13}C-depleted relative to calcite precipitated in equilibrium with seawater (Andres et al., 2006) and the $\delta^{13}C$ values of microbial micrite in biostalactites in a submarine cave off Belize (Gischler et al., 2017b) (Fig. 9). Carbon isotope values from LGM Reefs 2 and 3a are similar in the Hydrographer's and Noggin areas, and slightly higher than the values of the deglacial Reef 3b (Table S3). All examined microbialite fabrics, however, contain varying amounts of silt to sand-sized bioclasts (see Fig. 5b) and, therefore, the bulk-carbonate isotope values do not only reflect the composition of the microbial carbonate. As pointed out by Heindel et al. (2010), the measured bulk-carbonate $\delta^{13}C$ ratios are probably lower than the original ratios of "pure" microbial micrite because the incorporated bioclastic grains (corals, mollusks, etc.) are mainly aragonitic, with lower $\delta^{13}C$ values. The bulk-carbonate $\delta^{18}O$ values of microbialites in Reefs 2 and 3b are higher than those in Reef 3b (Table S3, Fig. 9) and generally higher than $\delta^{18}O$ values in deglacial and Holocene microbialites in Tahiti, Vanuatu and Belize (Camoin et al., 1999; Cabioch et al., 2006; Heindel et al., 2010; Gischler et al., 2017a), and modern micrite crusts in Bahamas and Belize (Andres et al., 2006; Gischler et al., 2017b). These higher values probably reflect lower seawater temperatures during the LGM than in later periods (Mix et al., 2001; Felis et al., 2014).

All microbialites contain siliciclastic grains (Table S2), mainly as clay fraction. In each transect there is no significant difference in siliciclastic content between reef phases. There is, however, a lower content of siliciclastics (3.3 to 8.5%, average 4.5%) in samples from HYD-01C than in those from NOG-01B (6.0 to 14.5%, average 9.8%). In the latter transect, quartz grains are recognizable in cores of Reefs 2 and 3a from the mid and outer terraces. The higher and coarser siliciclastic

Fig. 11. A. Gas chromatogram (total ion current) of the alcohol fraction from a GBR microbialite (GBR 2). B. Gas chromatogram (total ion current) of the fatty acid fraction from a GBR microbialite (GBR 2). Circles = *n*-alcohols and *n*-fatty acids; white triangles = *iso*- and *anteiso*-alcohols and fatty acids; black triangles = MAGEs (mono-*O*-alkyl glycerol ethers); C = contaminant; is = internal standard; *i* = *iso*, *ai* = *anteiso*.

content at NOG-01B is probably due to the large drainage system, 9 km south of the transect, that connected the emergent GBR shelf to the shelf-margin terraces during the LGM and early deglaciation (Abbey et al., 2011b), and to the narrower and steeper shelf edge in this location compared with that in Hydrographer's Passage (Hinestrosa et al., 2016).

5.2. Microbialite fabric succession

In the microbialites that formed on framework skeletons, the first fabric to develop is IBFM in intraskeletal spaces in corals (Fig. 10a) and invertebrate encrusters, as well as within frameworks of foliose CCA. It is roughly coeval with IBFM that infills the first generation of borings in the framework builders (Figs. 8a, 10a). The initial IBFM fabric is usually followed by microbial crusts, but as bioerosion continued during their accretion, new generations of borings were created and filled. The framework skeletons and first phase of IBFM are typically overlain by thin (usually < 1 cm) SM or LM crusts with diffuse lamination, which are commonly rich in large bioclasts and invertebrate encrusters and are intensely bioeroded (Figs. 7b, 10a). These crusts are usually overgrown by LM fabrics that locally terminate in a thin (< 1–2 cm) veneer of DM if the LM crust does not totally fill the empty space (Figs. 8b, 10a). MCD can appear at any stage of the succession, overlying the framework skeletons or intercalated within any of the other fabrics (Fig. 10). MCD can also be the last phase (Figs. 8d, 10b), but quite often the last available space is partially or completely filled by LM (locally plus DM), "unconformably" overlying other fabrics (i.e., lamina sets are oblique to the accretion surfaces of underlying microbialite). Bioerosion affects all phases of the succession (Fig. 10).

In other instances, especially in microbialite boundstones, there is no skeletal-framework substrate and microbialite develops on encrusting corals, centimeter-sized bioclasts or bioclastic accumulations (Fig. 10b). The fabric succession can be similar to that described above, or can be dominated by MCD alternating with crusts of any fabric.

Table 3
Contents of lipid biomarkers derived from sulfate-reducing bacteria (fatty acids and alcohols, ng lipid/g rock) and their compound-specific carbon isotopic values; tr = trace amounts; n.d. = not detected; n.m. = not measurable due to a combination of low peak intensities and co-elution. MAGE: mono-*O*-alkyl glycerol ether.

Transect	NOG-01B, Reef 3a (outer terrace)				NOG-01B, Reef 2 (inner terrace)	
Samples	GBR 2		GBR 4		GBR 3	
	(ng/g)	δ^{13}C (‰)	(ng/g)	δ^{13}C (‰)	(ng/g)	δ^{13}C (‰)
Compounds (fatty acids)						
iso-C$_{15}$	116	−21	185	−20	118	−21
anteiso-C$_{15}$	60	−23	113	−20	83	−22
10Me-C$_{16}$	30	n.m.	51	−20	69	n.m.
iso-C$_{17}$	64	−20	106	−20	65	−16
anteiso-C$_{17}$	32	n.m.	56	−22	39	−17
Compounds (alcohols)						
MAGE C$_{14}$	8	n.m.	14	−16	10	−16
MAGE *iso*-C$_{15}$	18	−18	20	−17	11	−17
MAGE C$_{15}$	5	n.m.	9	−19	11	−18
MAGE *iso*-C$_{16}$	3	n.m.	9	−17	4	n.m.
MAGE C$_{16}$	16	−16	29	−16	19	−14
MAGE *iso*-C$_{17}$	4	n.m.	6	−18	4	n.m.
MAGE *anteiso*-C$_{17}$	4	n.m.	8	−18	6	n.m.
MAGE C$_{17}$	5	n.m.	14	−16	12	−17
MAGE C$_{18}$	15	−17	21	−15	17	−16

Successions from laminated to digitate microbialites have been described in Tahiti deglacial reefs (Montaggioni and Camoin, 1993; Camoin and Montaggioni, 1994; Camoin et al., 1999; Westphal et al., 2010; Seard et al., 2011) and successions of IBFM-LM-DM can be recognized in published illustrations (e.g., Seard et al., 2011, Fig. 4A and B).

5.3. Paleoenvironments and timing of microbialite formation

The successive reef phases of the GBR during the LGM and deglaciation have been identified with the help of a dense framework of radiometric dates (Yokoyama et al., 2018; Webster et al., 2018) that reveal a complex stacking pattern controlled by sea-level variations during intervals of a few ka (Figs. 2 and 3). In addition, within each reef phase, the radiometric ages together with the coralgal assemblages facilitate paleoenvironmental and paleobathymetric reconstructions of reef deposits for short time slices (hundreds to thousand years). Isochrons depict the profiles of the reef system along each transect for any given time (Figs. 2 and 3), and the corresponding paleodepth of each deposit can be estimated by comparing its elevation with the highest coeval coralgal assemblages indicative of shallow-water described by Webster et al. (2018) and Humblet et al. (submitted). The degree of uncertainty affecting the paleodepth of shallow coralgal assemblages (5–10 m) is obviously transferred to the estimates for other reef facies, but does not alter their relative positions within reef environments.

For example, following a 15 ± 0.1 ka timeline in Reef 3b at transect HYD-01C (Fig. 2), microbialite in the inner terraces (M0033A 5) occurs as IBFM and as crusts on a framework of corals coated by CCA intergrown with vermetids. This coralgal assemblage is characteristic of shallow-water reef habitats (Webster et al., 2018). Microbialite crusts, a few centimeters thick, show a succession of IBFM-SM-LM-DM fabrics (Fig. 8b), and MCD occurs as relatively small and scattered accumulations. Coeval deposits in the outer terraces (M0039A 4) at an elevation 15 m lower (Fig. 2), comprise abundant MCD and pieces of coral that could be bioclasts within the breccia (Table 2). Both MCD accumulations and large coral pieces are coated by thin (< 1 cm) microbialite crusts, and both are affected by borings with IBFM infillings (Fig. 6).

In Reef 2, shallow-water reef deposits include microbialite that developed within both intraskeletal cavities and successive generations of borings, and as crusts on framework skeletons (coral and CCA/vermetids). Crusts can show an IBFM-SM-LM-(DM) fabric succession, and

Table 4
Calculated relative proportions of defined groups of alcohols and fatty acids in the rock samples GBR 1–4 (wt%), their mean compound-specific carbon isotopic values, and their potential source organisms. n.d. = not detected, n.m. = not measurable, tr = trace amounts. MAGE: mono-*O*-alkyl glycerol ether.

Sample	GBR 2		GBR 4		GBR 3		Averages	Source organisms
Relative proportions of defined groups of compounds in the rock (wt%)	(wt%)	δ^{13}C (‰)	(wt%)	δ^{13}C (‰)	(wt%)	δ^{13}C (‰)		
Short-chain *n*-fatty acids C$_{14–19}$	24	−25	31	−24	31	−24	29 wt% −24‰	Marine phyto-, zooplankton and bacteria (phototrophs, autotrophs, heterotrophs)
Short-chain *n*-fatty acids C$_{16:1\omega7}$, C$_{18:1\omega7}$, C$_{18:1\omega9}$	11	−25	9	−30	13	−29	11 wt% −28‰	Marine phyto-, zooplankton and bacteria (phototrophs, autotrophs, heterotrophs)
Brassica-, dino-, gorgosterol	4	−26	4	−21	1	−21	3 wt% −23‰	Marine phyto-, zooplankton and bacteria (phototrophs, autotrophs, heterotrophs)
Long-chain *n*-fatty acids C$_{25–33}$	7	−23	6	−23	13	−21	9 wt% −22‰	Higher land plants
Long-chain *n*-alcohols C$_{25–28}$	2	−25	1	−23	1	−23	1 wt% −24‰	Higher land plants
Stigma-, campe-, β-sitosterol, germanicol, lupeol	6	−26	6	−21	2	−21	5 wt% −23‰	Higher land plants
iso fatty acids C$_{16\ \&\ 18}$	1	−19	1	n.m.	1	n.m.	1 wt% −19‰	Unspecific bacteria
Hopanoic acids	4	−23	6	−23	4	n.m.	5 wt% −23‰	Unspecific bacteria
Bishomohopanol (17β(H),21β(H)-32-hopan-*ol*)	3	−20	3	−21	1	−20	2 wt% −20‰	Unspecific bacteria
iso/anteiso fatty acids C$_{15\ \&\ 17}$	5	−21	6	−21	4	−19	5 wt% −20‰	Sulfate-reducing bacteria
10-Me-C$_{16}$ fatty acid	1	n.m.	1	−20	1	n.m.	1 wt% −20‰	Sulfate-reducing bacteria
MAGE (*iso/anteiso*) C$_{14–18}$	1	−17	2	−17	1	−16	1 wt% −17‰	Sulfate-reducing bacteria

MCD is common and occurs intercalated on or within any other fabric but is not dominant. Coeval fore-reef deposits, 10–25 m deeper (Figs. 2 and 3), are microbialite boundstone dominated by crusts overlying encrusting corals and MCD. LM-(DM) crusts, several centimeters thick, developed on both MCD and on other crusts, as the final phase of microbialite succession (Table 1).

Similarly, in Reef 3a at transect NOG-01B, microbialites in shallow-water reef deposits grew within the cavernous structure created by framework builders, producing an IBFM-SM-LM-(DM) fabric succession with lenses of MCD. The coeval fore-reef deposits in the outer terrace formed some 10 m deeper (Figs. 2 and 3) and comprise microbialite boundstone dominated by crusts on intensely bioeroded encrusting corals with CCA and MCD (Table 1). In Reefs 3b and 4, microbialite in the shallow-water reef facies appears as IBFM and as thin crusts on corals and CCA, with intercalated patches of MCD. In fore-reef deposits, meters to tens of meters deeper, the recovered boundstone is dominated by MCD and LM (Table 2).

In short, fore-reef deposits that formed at a few meters to a few tens of meters depth in the GBR during the LGM and early deglaciation are characterized by bioclastic breccias with a "matrix" of microbial carbonate, and by encrusting corals and CCA coated by microbial crusts (Fig. 10b). Both corals and crusts were intensely bored during several phases of bioerosion. Intraskeletal spaces and borings are infilled by several generations of microbialite. The accretion of these fore-reef deposits took place by repeated superposition of MCD fabrics and encrusting corals/CCA overlain by crusts, and LM crusts developed on both (Fig. 8d). There was no cavernous coralgal framework prior to the formation of the microbial carbonate. On their own, encrusting corals (accounting for 5 to 25% of the boundstone volume) did not form significant frameworks and they typically occur as individual layers on the tops of microbialite intervals.

Consequently, the fore-reef microbialites formed on the sea floor, and in small cavities provided by larger bioclasts and encrusting corals in the top several centimeters of sediment, but not in cryptic habitats such as reef-framework cavities or caves. The estimated paleodepths for these fore-reef microbialite boundstones, a few meters to a few tens of meters (Webster et al., 2018) (Figs. 2 and 3), imply that they formed in the photic zone. The boundstone underwent early lithification, generating centimeter-scale spaces that were partially or totally filled by late microbialite deposits, usually showing LM-(DM) fabrics. Obviously, microbialite formation took place as the boundstone was accreting by the accumulation of bioclastic breccias and the growth of encrusting corals and CCA. Only the last microbialite phases, filling the empty boundstone spaces, perhaps represent late deposits that formed some time after the bulk of the fore-reef sediment. However, encrusting epibionts on the accretion surfaces of the laminae and the pervasive bioerosion suggest that the cavities infilled by these late microbialites were still in contact with seawater.

In contrast, coeval microbialites in shallow-water LGM and deglacial reef deposits in the GBR, which also occur as late stage veneers on framework skeletons, probably formed in framework cavities. They typically formed at the end of a succession of increasingly light-independent skeletal organisms: corals, shallow-water CCA and vermetids, sciaphilic CCA, followed by encrusting invertebrates such as vermetids, foraminifers, bryozoans and serpulids. Similar microbialites in deglacial shallow-water reefs in Tahiti have been interpreted as within euphotic zone reefs (Heindel et al., 2009), but developing 1.5 to 6 m below the top of the living reef (Seard et al., 2011; Camoin and Seard, 2012). Microbialites filling the cavernous framework in Tahiti shallow reefs have been interpreted to have formed either coevally with coral and CCA growth (Heindel et al., 2009) or up to a few hundred years after the coralgal communities (Seard et al., 2011; Camoin and Seard, 2012). This offset between the coralgal assemblages and associated microbialite crusts is deduced from the radiocarbon-age differences between microbial carbonates and the underlying corals and CCA. In the case of shallow-water reefs in the GBR, the common occurrence of

coarse-grained bioclastic accumulations within microbialite crusts, the abundant epibionts intergrown with the laminated crusts, and the persistent bioerosion of all phases of crust development (Figs. 7b and 8b), suggest that the cavities in which the microbialites accreted were in open contact with seawater, and may have been partially illuminated.
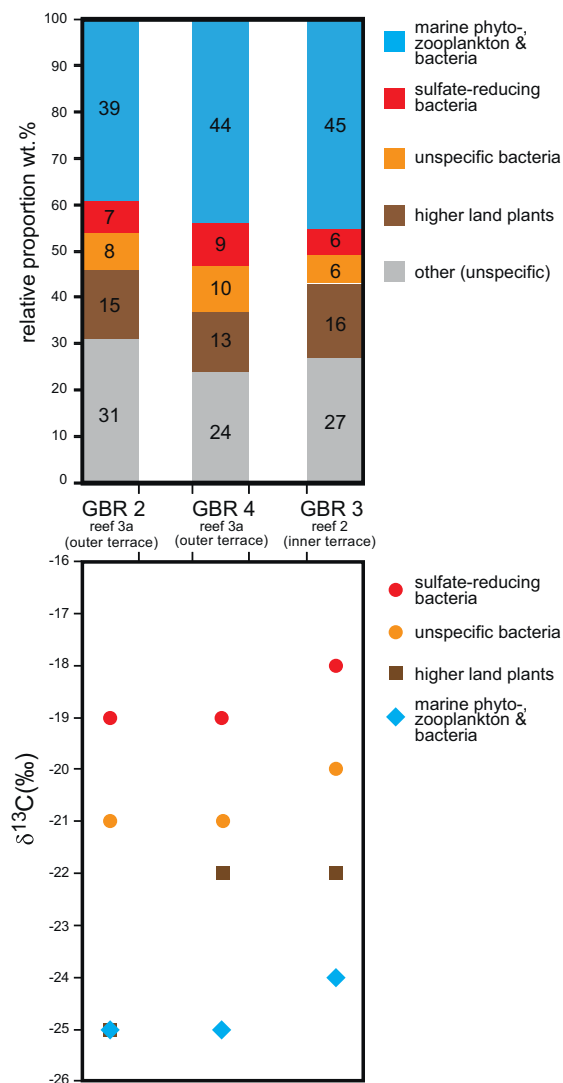
5.4. Evidence for sulfate-reducing bacteria and reconstruction of the deglacial carbon pool

The inventory of lipid biomarkers found in the GBR microbialites (especially the inventory of bacterial-derived compounds) resembles that of other last-deglacial reefal microbialites (Heindel et al., 2012) and other shallow-marine microbialites from cryptic environments (Guido et al., 2013; Gischler et al., 2017a, b). A range of compounds of intermediate to high specificity for sulfate-reducing bacteria (*iso-* and *anteiso*-$C_{15/17}$ fatty acids, 10Me-C_{16} fatty acid, MAGEs) was detected in the microbialites from all GBR study sites. Similar to reefal microbialites of Tahiti, Vanuatu, Belize and the Maldives (Heindel et al., 2012), biomarkers of cyanobacteria were not detected in the GBR microbialites, irrespective of the inferred formation depth including photic environments. This observation does not necessarily indicate the absence of cyanobacteria, but it suggests that cyanobacteria were probably not directly involved in the formation of microbialites (cf., Heindel et al., 2010). In accordance with previous studies on other reefal microbialites (Heindel et al., 2010, 2012) and microbialites from cryptic shallow-water environments, the new lipid biomarker data set points to sulfate-reducing bacteria as critical agents in microbialite formation. Because the carbon stable isotope patterns of these different microbialites disagree with substantial carbonate production from the remineralization of organic matter, it is likely that matrix effects related to the EPS of sulfate-reducing bacteria rather than metabolism favored carbonate precipitation.

The circumstance that the lipids assigned to sulfate-reducing bacteria revealed higher $\delta^{13}C$ values (average: −19‰; Fig. 12) than the biomarkers derived from land plants (average: −23‰) and other marine organisms (average: −25‰), also agrees with patterns of other reefal microbialites (Heindel et al., 2010, 2012) and other shallow-water microbialites (Guido et al., 2013). This relationship was previously interpreted to reflect ^{13}C enrichment due to enzymatic isotope fractionation by sulfate-reducing bacteria (cf. Londry and Des Marais, 2003; Heindel et al., 2010), possibly combined with the consumption of relatively ^{13}C enriched biomass such as carbohydrates, proteins and peptides (Heindel et al., 2012) all abundant constituents of bacterial EPS (e.g., Decho, 1990).

The highest content of land-plant derived biomarkers (16 wt%) in the microbialite from Reef 2 might be due to increased erosional input of terrestrial detritus during subaerial exposure of Reef 2 at lowest sea level (growth of Reef 3a). According to the hiatus recorded in Hole M0055A from the top of core 4, the top of Reef 2 was exposed for about 5 ka (from 22 to 16.5 ka). Another explanation could be the transport of terrestrial material including land plants to the shallow-water reef by the large drainage system, located 9 km south of the transect NOG-01B, that connected the emergent GBR shelf to the shelf-margin terraces during the LGM and early deglaciation (Abbey et al., 2011b).

Microbialite formation driven by sulfate-reducing bacteria took place in anoxic microenvironments (Heindel et al., 2012), probably favored by high nutrient levels and resultant accumulation of organic matter (Camoin et al., 1999, 2006; Heindel et al., 2012). The high amounts of ascidian spicules within all microbialite fabrics (Figs. 4a, e, and 5a) support high productivity of reef waters, as the ascidians are typical suspension feeders that thrive in fertilized marine environments. During the LGM and deglaciation the shelf-edge terraces of the GBR were under the influence of rivers draining the Northeast Australian shelf, as indicated by the siliciclastic content of the microbial carbonates and the biomarkers showing a strong input from land plants. As in

Fig. 12. A. Comparison of distribution patterns (in relative percentages: wt%) of lipid biomarkers in the three GBR microbialites (GBR 2–4). B. Compound-specific $\delta^{13}C$ values of specific fatty acids and alcohols assigned to groups of specific organisms (sulfate-reducing bacteria, unspecific bacteria, higher land plants, and marine phytoplankton, zooplankton and bacteria) in the GBR microbialites.

other geological settings of deglacial reef microbialite formation (Belize, Maldives), the fertilization of waters cannot be attributed to weathering of a volcanic hinterland only (Heindel et al., 2012), which was previously suggested to explain microbialite development in postglacial reefs off Tahiti and Vanuatu (Camoin et al., 1999; Cabioch et al., 2006; Heindel et al., 2010). In any case, decomposition of organic matter in reef frameworks can produce nutrient-rich interstitial waters (Riding et al., 2014 and references therein).

In the GBR, microbialite development was volumetrically at its highest during the LGM and early deglaciation (Reefs 2 and 3a), from 28 to 16.5 ka, and decreased in later deglacial reef phases (Reefs 3b and 4) (Figs. 2 and 3). This trend cannot readily be explained by higher fertilization levels due to higher weathering, precipitation and subsequent run-off, or by the existence of larger drainage basins in the Northeast Australian shelf during the LGM and early deglaciation. Increased weathering and run-off were unlikely as the LGM climate was cooler and drier at low latitudes (Otto-Bliesner et al., 2006), and the increase of the exposed area during the lowest sea level in relation to later phases of deglaciation until reflooding of the shelf would only

minimally increase the proportion of exposed surface. For example, in the Noggin area the exposed surface of shelf and shelf edge at −130 m, the minimum possible sea level recorded by Reef 3a (Webster et al., 2018), is only 0.5% greater than that at −100 m (Hinestrosa et al., 2014), which was the sea-level position at the beginning of Reef 3b growth. In addition, the large gamma spikes in core logs, indicating higher siliciclastic fluxes, occur after the LGM at about 15–16 ka (Webster et al., 2018).

The increased development of microbialite during the LGM and early deglaciation that we observe can plausibly be related to higher seawater carbonate saturation in response to lower levels of atmospheric CO_2. Riding et al. (2014) proposed that fluctuations in tropical seawater pH over Quaternary glacial cycles could have been sufficient to markedly increase reef microbialite formation during glacial periods, and reduce their formation during interglacials. Thus, in addition to accounting for the widespread deglacial decline (Camoin et al., 1999) noted in reef microbialites, this effect of seawater chemistry on microbialite formation is consistent with increase in the volume of microbialites during the last glaciation at the GBR.

6. Conclusions

Microbial carbonate crusts are significant constituents of Last Glacial Maximum and deglacial reef deposits in the Australian Great Barrier Reef. They are major components in coralgal-microbialite and microbialite boundstones, and form minor veneers on the framework builders in coralgal boundstone. They consist of varying proportions of micrite/microspar, allochthonous bioclastic and siliciclastic particles, fenestrae and encrusting epibionts. Under ESEM the micrite consists of aggregates of small (< 1 μm to a few micrometers) blocky crystals of high-magnesian calcite. An intraskeletal and boring-fill microbialite fabric is the first to develop in skeletal voids and bioerosion cavities in the coralgal framework. It is usually followed by a succession of structureless or laminated microbialite fabrics, locally ending with a digitate fabric. Microbialite-coated debris occurs in pockets on any fabric in this succession and can also be the main fabric in microbialite boundstones. All fabrics are affected by several phases of bioerosion, resulting in repeated generations of boring-filling microbialite, or empty borings.

The lipid biomarkers in these microbialites have consistently high compound-specific $\delta^{13}C$ values indicating that sulfate-reducing bacteria promoted microbialite formation in anoxic microenvironments. A significant amount of microbialite formed within and on bioclastic breccias with sparse encrusting corals in fore-reef paleoenvironments, at depths of a few meters to a few tens of meters, on the sea floor in the photic zone, and in small spaces provided by bioclasts and encrusting corals in the topmost centimeters of sediment. These microbial coatings were essentially coeval with associated debris, corals and other encrusters. This photic-zone microbialite contrasts with the cryptic crusts previously reported from cavities in shallow-water deglacial reefs and from deeper fore-reef settings. Microbialite in all reef phases probably developed under high nutrient levels. The maximum development of microbial crusts in the Great Barrier Reef, however, occurs in reefs from the LGM and early deglacial interval (28 to 16 ka). This is consistent with microbialite formation being favored by higher carbonate saturation of seawater during glacial and early deglacial intervals when levels of atmospheric CO_2 were lower than during the Holocene.

Supplementary data to this article can be found online at https://doi.org/10.1016/j.palaeo.2018.10.007.

References

Abbey, E., Webster, J.M., Beaman, R.J., 2011a. Geomorphology of submerged reefs on the shelf edge of the Great Barrier Reef: the influence of oscillating Pleistocene sea levels. Mar. Geol. 288, 61–78.

Abbey, E., Webster, J.M., Braga, J.C., Sugihara, K., Wallace, C.C., Iryu, Y., Potts, D., Done, T., Camoin, G., Seard, C., 2011b. Variation in deglacial coralgal assemblages and their paleoenvironmental significance: IODP Expedition 310, "Tahiti Sea Level". Glob. Planet. Chang. 76, 1–15.

Albers, C.S., Kattner, G., Hagen, W., 1996. The compositions of wax esters, triacylglycerols and phospholipids in Arctic and Antarctic copepods: evidence of energetic adaptations. Mar. Chem. 55, 347–358.

Andres, M.S., Sumner, D.Y., Reid, R.P., Swart, P.K., 2006. Isotopic fingerprints of microbial respiration in aragonite from Bahamian stromatolites. Geology 34, 973–976.

Birgel, D., Elvert, M., Han, X., Peckmann, J., 2008. ^{13}C-depleted biphytanic diacids as tracers of past anaerobic oxidation of methane. Org. Geochem. 39, 152–156.

Boon, J.J., Rijpstra, W.I.C., De Lange, F., De Leeuw, J.W., Yoshioka, M., Shimizu, Y., 1979. The Black Sea sterol: a molecular fossil for dinoflagellate blooms. Nature 277, 125–127.

Brachert, T.C., Dullo, W.C., 1991. Laminar micrite crusts and associated foreslope processes, Red Sea. J. Sediment. Res. 61, 354–363.

Burne, R.V., Moore, L.S., 1987. Microbialites: organosedimentary deposits of benthic microbial communities. Palaios 2, 241–254.

Cabioch, G., Taylor, F.W., Récy, J., Edwards, R.L., Gray, S.C., Faure, G., Burr, G.S., Corrège, T., 1998. Environmental and tectonic influences on growth and internal structure of a fringing reef at Tasmaloum (South West Espiritu Santo, New Hebrides Island Arc, South West Pacific). In: Camoin, G., Davies, P.J. (Eds.), Reefs and Carbonate Platforms of the Pacific and Indian Ocean Spec. Publ. Int. Ass. Sedimentol. vol. 25. pp. 261–277.

Cabioch, G., Camoin, G.F., Montaggioni, L.F., 1999a. Postglacial growth history of a French Polynesian barrier reef tract, Tahiti, central Pacific. Sedimentology 46, 985–1000.

Cabioch, G., Taylor, F.W., Corrège, T., Récy, J., Edwards, L.R., Burr, G.S., Le Cornec, F., Banks, K.A., 1999b. Occurrence and significance of microbialites in the uplifted Tasmaloum reef (SW Espiritu Santo, SW Pacific). Sediment. Geol. 126, 305–316.

Cabioch, G., Camoin, G., Webb, G.E., Le Cornec, F., Molina, M.G., Pierre, C., Joachimski, M.M., 2006. Contribution of microbialites to the development of coral reefs during the last deglacial period: case study from Vanuatu (south-west Pacific). Sediment. Geol. 185, 297–318.

Camoin, G.F., Montaggioni, L.F., 1994. High energy coralgal-stromatolite frameworks from Holocene reefs (Tahiti, French Polynesia). Sedimentology 41, 655–676.

Camoin, C., Seard, C., 2012. Genesis of microbialites as contemporaneous framework components of deglacial coral reefs, Tahiti (IODP 310): COMMENT. Facies 58, 163–165.

Camoin, G.F., Colonna, M., Montaggioni, L.F., Casanova, J., Faure, G., Thomassin, B.A., 1997. Holocene sea level changes and reef development in southwestern Indian Ocean. Coral Reefs 16, 247–259.

Camoin, G.F., Gautret, P., Montaggioni, L.F., Cabioch, G., 1999. Nature and environmental significance of microbialites in Quaternary reefs: the Tahiti paradox. Sediment. Geol. 126, 271–304.

Camoin, G.F., Cabioch, G., Eisenhauer, A., Braga, J.-C., Hamelin, B., Lericolais, G., 2006. Environmental significance of microbialites in reef environments during the last deglaciation. Sediment. Geol. 185, 277–295.

Decho, A.W., 1990. Microbial exopolymer secretions in ocean environments: their role(s) in food webs and marine processes. Oceanogr. Mar. Biol. Annu. Rev. 28, 73–153.

Edlund, A., Nichols, P.D., Roffky, R., White, D.C., 1985. Extractable and lipopolysaccharide fatty acid and hydroxy acid profiles from *Desulfovibrio* species. J. Lipid Res. 29, 982–988.

Eglinton, G., Hamilton, R.J., 1967. Leaf epicuticular waxes. Science 156, 1322–1335.

Eglinton, G., Hunnemann, D.H., Douraghi-Zadeh, K., 1968. Gas-chromatographic-mass spectrometric studies of long chain hydroxy acids: II. The hydroxy acids and fatty acids of a 5000 year old lacustrine sediment. Tetrahedron 24, 5929–5941.

Elvert, M., Boetius, A., Knittel, K., Jørgensen, B.B., 2003. Characterization of specific membrane fatty acids as chemotaxonomic markers for sulfate-reducing bacteria involved in anaerobic oxidation of methane. Geomicrobiol J. 20, 403–419.

Felis, T., McGregor, H.V., Linsley, B.K., Tudhope, A.W., Gagan, M.K., Suzuki, A., Inoue, M., Thomas, A.L., Esat, T.M., Thompson, W.G., Tiwari, M., Potts, D.C., Mudelsee, M., Yokoyama, Y., Webster, J.M., 2014. Intensification of the meridional temperature gradient in the Great Barrier Reef following the Last Glacial Maximum. Nat. Commun. 5, 4102.

Gischler, E., Birgel, D., Brunner, B., Eisenhauer, A., Meyer, G., Buhre, S., Peckmann, J., 2017a. A giant underwater, encrusted stalactite from the Blue Hole, Lighthouse Reef, Belize, revisited: a complex history of biologically induced carbonate accretion under changing meteoric and marine conditions. J. Sediment. Res. 87, 1260–1284.

Gischler, E., Heindel, K., Birgel, D., Brunner, B., Reitner, J., Peckmann, J., 2017b. Cryptic biostalactites in a submerged karst cave of the Belize Barrier Reef revisited: Pendant bioconstructions cemented by microbial micrite. Palaeogeogr. Palaeoclimatol. Palaeoecol. 468, 34–51.

Graeve, M., Kattner, G., Piepenburg, D., 1997. Lipids in Arctic benthos: does the fatty acid and alcohol composition reflect feeding and trophic interactions? Polar Biol. 18, 53–61.

Grossi, V., Mollex, D., Vinçon-Laugier, A., Hakil, F., Pacton, M., Cravo-Laureau, C., 2015. Mono- and dialkyl glycerol ether lipids in anaerobic bacteria: Biosynthetic insights from the mesophilic sulfate reducer *Desulfatibacillum alkenivorans* PF 2803T. Appl. Environ. Microbiol. 81, 3157–3168.

Guido, A., Heindel, K., Birgel, D., Rosso, A., Mastandrea, A., Sanfilippo, R., Russo, F., Peckmann, J., 2013. Pendant bioconstructions cemented by microbial carbonate in submerged marine caves (Holocene, SE Sicily). Palaeogeogr. Palaeoclimatol. Palaeoecol. 388, 166–180.

Heindel, K., Wisshak, M., Westphal, H., 2009. Microbioerosion in Tahitian reefs: a record of environmental change during the last deglacial sea-level rise (IODP 310). Lethaia 42, 322–340.

Heindel, K., Birgel, D., Peckmann, J., Kuhnert, H., Westphal, H., 2010. Formation of deglacial microbialites in coral reefs off Tahiti (IODP 310) involving sulfate-reducing bacteria. Palaios 25, 618–635.

Heindel, K., Birgel, D., Brunner, B., Thiel, V., Westphal, H., Gischler, E., Ziegenbalg, S.B., Cabioch, G., Sjövall, P., Peckmann, J., 2012. Post-glacial microbialite formation in coral reefs in the Pacific, Atlantic, and Indian Oceans. Chem. Geol. 304–305, 117–130.

Hinestrosa, G., Webster, J.M., Beaman, R.J., Anderson, L., 2014. Seismic stratigraphy and development of the shelf-edge reefs of the Great Barrier Reef, Australia. Mar. Geol. 353, 1–20.

Hinestrosa, G., Webster, J.M., Beaman, R.J., 2016. Postglacial sediment deposition along a mixed carbonate-siliciclastic margin: new constraints from the drowned shelf-edge reefs of the Great Barrier Reef, Australia. Palaeogeogr. Palaeoclimatol. Palaeoecol. 446, 168–185.

Humblet, M., Potts, D.C., Webster, J.M., Braga, J.C., Iryu, Y., Yokoyama, Y., Bourillot, R., Seard, C., Droxler, A., Fujita, K., Gischler, E., Kan, H., 2018. Late glacial to deglacial variation of coralgal assemblages in the Great Barrier Reef, Australia. Glob. Planet. Chang (submitted for publication).

Kaneda, T., 1991. Iso- and anteiso-fatty acids in bacteria: biosynthesis, function, and taxonomic significance. Microbiol. Rev. 55, 288–302.

Koch, B.P., Souza Filho, P.W.M., Behling, H., Cohen, M.C.L., Kattner, G., Rullkötter, J., Scholz-Böttcher, B., Lara, R.J., 2011. Triterpenols in mangrove sediments as a proxy for organic matter derived from the red mangrove (*Rhizophora mangle*). Org. Geochem. 42, 62–73.

Langworthy, T.A., Holzer, G., Zeikus, J.G., Tornabene, T.G., 1983. Iso- and anteiso branched glycerol diethers of thermophilic anaerobe *Thermodesulfotobacterium commune*. Syst. Appl. Microbiol. 4, 1–17.

Londry, K.L., Des Marais, D.J., 2003. Stable carbon isotope fractionation by sulfate-reducing bacteria. Appl. Environ. Microbiol. 69, 2942–2949.

Macintyre, I.G., 1977. Distribution of submarine cements in a modern Caribbean Fringing Reef, Galeta Point, Panama. J. Sediment. Petrol. 47, 503–516.

Macintyre, I.G., 1984. Extensive submarine lithification in a cave in the Belize Barrier Reef Platform. J. Sediment. Petrol. 54, 221–235.

Marshall, J.F., Davies, P.J., 1981. Submarine lithification on windward reef slopes: Capricorn-Bunker Group, southern Great Barrier Reef. J. Sediment. Petrol. 51, 953–960.

Mix, A.C., Bard, E., Schneider, R., 2001. Environmental processes of the ice age: land, oceans, glaciers (EPILOG). Quat. Sci. Rev. 20, 627–657.

Moldowan, J.M., Jacobson, S.R., 2000. Chemical signals for early evolution of major taxa: biosignatures and taxon-specific biomarkers. Int. Geol. Rev. 42, 805–812.

Montaggioni, L.F., Camoin, G.F., 1993. Stromatolites associated with coralgal communities in Holocene high energy reefs. Geology 21, 149–152.

Otto-Bliesner, B.L., Brady, E.C., Clauzet, G., Tomas, R., Levis, S., Kothavala, Z., 2006. Last Glacial Maximum and Holocene climate in CCSM3. J. Clim. 19, 2526–2544.

Parkes, R.J., Taylor, J., 1983. The relationship between fatty acid distributions and bacterial respiratory types in contemporary marine sediments. Estuar. Coast. Shelf Sci. 16, 173–189.

Pigott, J.D., Land, L.S., 1986. Interstitial water chemistry of Jamaican reef sediment: sulfate reduction and submarine cementation. Mar. Chem. 19, 355–378.

Pratt, B.R., 1982. Stromatolite decline, a reconsideration. Geology 10, 512–515.

Rampen, S.W., Volkman, J.K., Hur, S.B., Abbas, B.A., Schouten, S., Jameson, I.D., Holdsworth, D.G., Hee Bae, J., Sinninghe Damsté, J.S., 2009. Occurrence of gorgosterol in diatoms of the genus *Delphineis*. Org. Geochem. 40, 144–147.

Reitner, J., Thiel, V., Zankl, H., Michaelis, W., Worheide, G., Gautret, P., 2000. Organic and biogeochemical patterns in cryptic microbialites. In: Riding, R., Awramik, S.M. (Eds.), Microbial Sediments. Springer, Berlin, pp. 149–160.

Riding, R., 2011a. Reefal microbial crusts. In: Hopley, D. (Ed.), Encyclopedia of Modern Coral Reefs. Encyclopedia of Earth Science Series Springer, Heidelberg, pp. 911–915.

Riding, R., 2011b. Microbialites, stromatolites, and thrombolites. In: Reitner, J., Thiel, V. (Eds.), Encyclopedia of Geobiology. Encyclopedia of Earth Science Series Springer, Heidelberg, pp. 635–654.

Riding, R., Tomás, S., 2006. Stromatolite reef crusts, Early Cretaceous, Spain: bacterial origin of in situ precipitated peloid microspar? Sedimentology 53, 23–34.

Riding, R., Martín, J.M., Braga, J.C., 1991. Coral stromatolite reef framework, Upper Miocene, Almeria, Spain. Sedimentology 38, 799–818.

Riding, R., Liang, L., Braga, J.C., 2014. Millennial-scale ocean acidification and late Quaternary decline of cryptic bacterial crusts in tropical reefs. Geobiology 12, 387–405.

Romano, I., Finore, I., Nicolaus, G., Huertas, F.J., Lama, L., Nicolaus, B., Poli, A., 2008.

Halobacillus alkaliphilus sp nov., a halophilic bacterium isolated from a salt lake in Fuente de Piedra, southern Spain. Int. J. Syst. Evol. Microbiol. 58, 886–890.

Rütters, H., Sass, H., Cypionka, H., Rullkötter, J., 2001. Monoalkylether phospholipids in the sulfate-reducing bacteria *Desulfosarcina variabilis* and *Desulforhabdus amnigenus*. Arch. Microbiol. 176, 435–442.

Seard, C., Camoin, G.F., Yokoyama, Y., Matsuzaki, H., Durand, N., Bard, E., Sepulcre, S., Deschamps, P., 2011. Microbialite development patterns in the last deglacial reefs from Tahiti (French Polynesia; IODP expedition #310): implications on reef framework architecture. Mar. Geol. 279, 63–86.

Taylor, J., Parkes, R.J., 1983. The cellular fatty acids of the sulfate-reducing bacteria *Desulfobacter* sp., *Desulfobulbus* sp. and *Desulfovibrio desulfuricans*. Journal of Genetic. Microbiology 129, 3303–3309.

Vinçon-Laugier, A., Grossi, V., Pacton, M., Escarguel, G., Cravo-Laureau, C., 2016. The alkyl glycerol ether lipid composition of heterotrophic sulfate reducing bacteria strongly depends on growth substrate. Org. Geochem. 98, 141–154.

Vinçon-Laugier, A., Cravo-Laureau, C., Mitteaus, I., Grossi, V., 2017. Temperature-dependent alkyl glycerol ether lipid composition of mesophilic and thermophilic sulfate-reducing bacteria. Front. Microbiol. 8, 1532. https://doi.org/10.3389/fmicb.2017.01532.

Vinçon-Laugier, A., Cravo-Laureau, C., Grossi, V., 2018. Selective preservation among bacterial alkyl glycerol ether lipid structures during long term oxic and anoxic incubation. Org. Geochem. 125, 24–28.

Volkman, J.K., 1986. A review of sterol markers for marine and terrigenous organic matter. Org. Geochem. 9, 83–99.

Volkman, J.K., Jeffrey, S.W., Nichols, P.D., Rogers, G.I., Garland, C.D., 1989. Fatty acid and lipid composition of 10 species of microalgae used in mariculture. J. Exp. Mar. Biol. Ecol. 128, 219–240.

Volkman, J.K., Barrett, S.M., Dunstan, G.A., Jeffrey, S.W., 1993. Geochemical significance

of the occurrence of dinosterol and other 4-methyl sterols in a marine diatom. Org. Geochem. 20, 7–15.

Webb, G.E., 1996. Was Phanerozoic reef history controlled by the distribution of nonenzymatically secreted reef carbonates (microbial carbonate and biologically induced cement)? Sedimentology 43, 947–971.

Webster, J.M., Braga, J.C., Clague, D.A., Gallup, C., Hein, J.R., Potts, D.C., Renema, W., Riding, R., Riker-Coleman, K., Silver, E., Wallace, L.M., 2009. Coral reef evolution on rapidly subsiding margins. Glob. Planet. Chang. 66, 129–148.

Webster, J.M., Yokoyama, Y., Cotterill, C., the Expedition 310 Scientists, 2011. Proceedings of the IODP. 325 Integrated Ocean Drilling Program Management International, Inc, Tokyo.

Webster, J.M., Braga, J.C., Humblet, M., Potts, D.C., Iryu, Y., Yokoyama, Y., Fujita, K., Bourillot, R.M., Esat, T.M., Fallon, S., Thompson, W.G., Thomas, A.L., Kan, H., McGregor, H.V., Hinestrosa, G., Obrochta, S.P., Lougheed, B.C., 2018. Response of the Great Barrier Reef to sea-level and environmental changes over the past 30,000 years. Nat. Geosci. 11, 426–433.

Westphal, H., Heindel, K., Brandano, M., Peckmann, J., 2010. Genesis of microbialites as contemporaneous framework components of coral reefs, deglacial of Tahiti (IODP 310). Facies 56, 337–352.

Yokoyama, Y., Webster, J.M., Cotterill, C., Braga, J.C., Jovane, L., Mills, H., Morgan, S., Suzuki, A., 325 Scientists, Expedition, 2011. IODP Expedition 325: Great Barrier Reefs reveals past sea-level, climate and environmental changes since the last Ice Age. Sci. Drill. 12, 32–45.

Yokoyama, Y., Esat, T.M., Thompson, W.G., Thomas, A.L., Webster, J.M., Miyairi, Y., Sawada, C., Aze, T., Matsuzaki, H., Okuno, J., Fallon, Stewart, Braga, J.C., Humblet, M., Iryu, Y., Potts, D.C., Fujita, K., Suzuki, A., Kan, H., 2018. Rapid glaciation and a two-step sea level plunge into the Last Glacial Maximum. Nature 559, 603–607.